Aus der Medizinischen Klinik der Universität Heidelberg

(Zentrumssprecher: Prof. Dr. med. Hugo A. Katus)

Abteilung für Innere I und Klinische Chemie

(Ärztlicher Direktor: Prof. Dr. med. Dr. h.c. Peter P. Nawroth)

Diabetes-induced mitochondrial changes are tissue- and model-dependent and elevated glucose levels do not activate the pathways of hyperglycemic damage in the kidney

Inauguraldissertation zur Erlangung

des Doctor scientiarum humanarum

an der Medizinischen Fakultät Heidelberg

der Ruprecht-Karls-Universität

vorgelegt von

Nadine Volk

geboren in Eberbach am Neckar

Heidelberg, 2016

Dekan: Prof. Dr. med. Wolfgang Herzog

Doktorvater: Prof. Dr. med. Dr. h. c. Peter P. Nawroth

Betreuer: Dr. sc. hum. Thomas H. Fleming

Table of contents

Table of contents

1 Abbreviations

1,3-bPG	1,3-bisphosphoglycerat
ADPR	ADP-ribose
AGE	Advanced glycation endproduct
B2m	Beta-2 microglobulin
Cat	Catalase
CoQ	Coenzyme Q
Ctrl	Control
DAG	Diacylglycerol
DHAP	Dihydroxyacetone phosphate
ETC	Electron transport chain
FAD(H$_2$)	Flavin adenine dinucleotide
FMN	Flavin mononucleotice
Fruc-1,6-bP	Fructose-1,6-bisphosphat
Fruc-6-P	Fructose-6-phosphat
GAP(DH)	Glyceraldehyde 3-phosphate (dehydrogenase)
Glo	Glyoxalase
Glu-6-P	Glucose-6-phosphat
Gpx	Glutathione peroxidase
HFD	High fat diet
Hprt	Hypoxanthine guanine phosphoribosyl transferase
IHC	Immunohistochemistry
MG	Methylglyoxal
MRS	Magnetic resonance spectroscopy
mt	Mitochondrium
NA	Nicotinic acid
NAD(H)	Nicotinamide adenine dinucleotide
NADP(H)	Nicotinamide adenine dinucleotide phosphate
NNT	Number needed to treat
Nqo1	NAD(P)H quinone reductase
Nrf2	Nuclear factor, erythroid derived 2, like 2
O-GlcNAc	O-Linked β-N-acetylglucosamine
PARP	Poly(ADP-ribose) polymerase
PKC	Protein kinase C
Polr2b	Polymerase (RNA) II (DNA directed) polypeptide B
Rn18s	18S ribosomal RNA
ROS	Reactive oxygen species
Sod	Superoxide (O_2^-) dismutase
STZ	Streptozotocin
T1D	Type 1 diabetes
T2D	Type 2 diabetes
Tbp	TATA box binding protein
TCA	Tricarboxylic acid
Ywhaz	Tyrosine 3-monooxygenase

2 Introduction

2.1 What is diabetes?

Diabetes mellitus is a disorder of glucose homeostasis, which is characterized by hyperglycemia. There are different forms of diabetes with the most important forms type 1 and type 2.

Type 1 diabetes (T1D), previously known as juvenile diabetes, is typically diagnosed before the age of 30 and accounts for about 5 % of the diabetic patients (Daneman, 2006). Destruction and loss of the β-cells in the pancreas causes insulin-deficiency resulting in many changes in the organism, including hyperglycemia (Alberti and Zimmet, 1998). The mechanism for the loss of β-cells is not fully understood, however, it has been suggested that an autoimmune response resulting from a combination of genetic and environmental factors, may be the drive force (Davies et al., 1994). Patients require regular exogenous insulin administration to control their blood glucose levels.

Type 2 diabetes (T2D), in contrast to T1D, is characterized by the loss of insulin sensitivity. The exact mechanism for the development of T2D is not fully understood. The pathogenesis seems to be correlated to increased secretion of inflammatory cytokines leading to peripheral insulin resistance in particular in the liver and muscle (Cai et al., 2005; Spranger et al., 2003). To compensate, the secretion of insulin is enhanced (hyposecretion). However, the regulatory mechanism against insulin resistance declines over time due to malfunction of the pancreas resulting in consecutive hyperglycemia. Depending on the extent of insulin resistance, patients with T2D are treated with several drugs including metformin, which improves insulin signaling and other drugs such as sulfonylurea and glifozins which stimulate insulin secretion and glucose excretion in the kidney (Kahn et al., 2014; Maruthur et al., 2016).

Both types of diabetes are associated with long-term complications, which are classically subdivided into macrovascular complications (such as cardiovascular disease, stroke, cardiac infarction) and microvascular complications (such as retinopathy, nephropathy, neuropathy). There is also evidence for vascular-

independent development of neuropathy (Bierhaus et al., 2012; Eberhardt et al., 2012). Currently, the exact mechanisms involved in the development of diabetic complications are still not fully understood.

2.2 Can the unifying theory explain diabetic complications?

It is commonly accepted that hyperglycemia constitutes the very origin in the development of diabetic complications. This hypothesis, referred to as the unifying theory, is supported by the fact that diabetic complications occur in tissues that take in glucose independently from the insulin concentration in the blood, such as mesangial cells in the kidney, capillary endothelial cells in the retina, as well as neurons and Schwann cells (Brownlee, 2001; Coughlan et al., 2007). During periods of hyperglycemia, these cells internalize large amounts of glucose, causing supranormal intracellular glucose concentrations. The accumulation of glucose leads to increased formation of reactive oxygen species (ROS) in the mitochondria. This activates the polyol pathway, the hexosamine pathway as well as protein kinase C (and subsequently NFκB) and increases the formation of advanced glycation endproducts (AGEs), (Figure 1). It has been suggested that the activation of all four pathways together gives rise to the cellular dysfunction in diabetes and the subsequent development of complications (Brownlee, 2001, 2005; Giacco and Brownlee, 2010).

The pathways of cellular dysfunction in the unifying theory

The accumulation of glucose and the subsequent increase in metabolic flux through glycolysis results in increased levels of substrates for the tricarboxylic acid (TCA) cycle and oxidative phosphorylation, leading to increased electron flux in the electron transport chain (ETC) and overproduction of ROS in the mitochondria. Superoxide (O_2^-) is the initial ROS formed, but it can be converted into other reactive species (see 2.3). If the load of O_2^- exceeds the antioxidant capacity of the cell, it diffuses into the nucleus where it causes double strand breaks to the DNA. It is, however, not feasible to reliably estimate the levels of O_2^- produced by the mitochondria *in vivo* (Murphy, 2009). As such, the concentrations, which are required to generate oxidative damage to the DNA, remain unknown. Nevertheless,

Introduction

it has been shown, that ROS-induced DNA damage activates the poly(ADP-ribose) polymerase (PARP), an enzyme involved in DNA repair (Atorino et al., 2001; Du et al., 2003; de Murcia et al., 1997). PARP breaks down nicotinamide adenine dinucleotide (NAD$^+$) into nicotinic acid (NA) and ADP-ribose (ADPR), then produces polymers of ADPR and transfers them to glyceraldehyde 3-phosphate dehydrogenase (GAPDH) thereby deactivating the enzyme (Du et al., 2003; Kanwar and Kowluru, 2009).
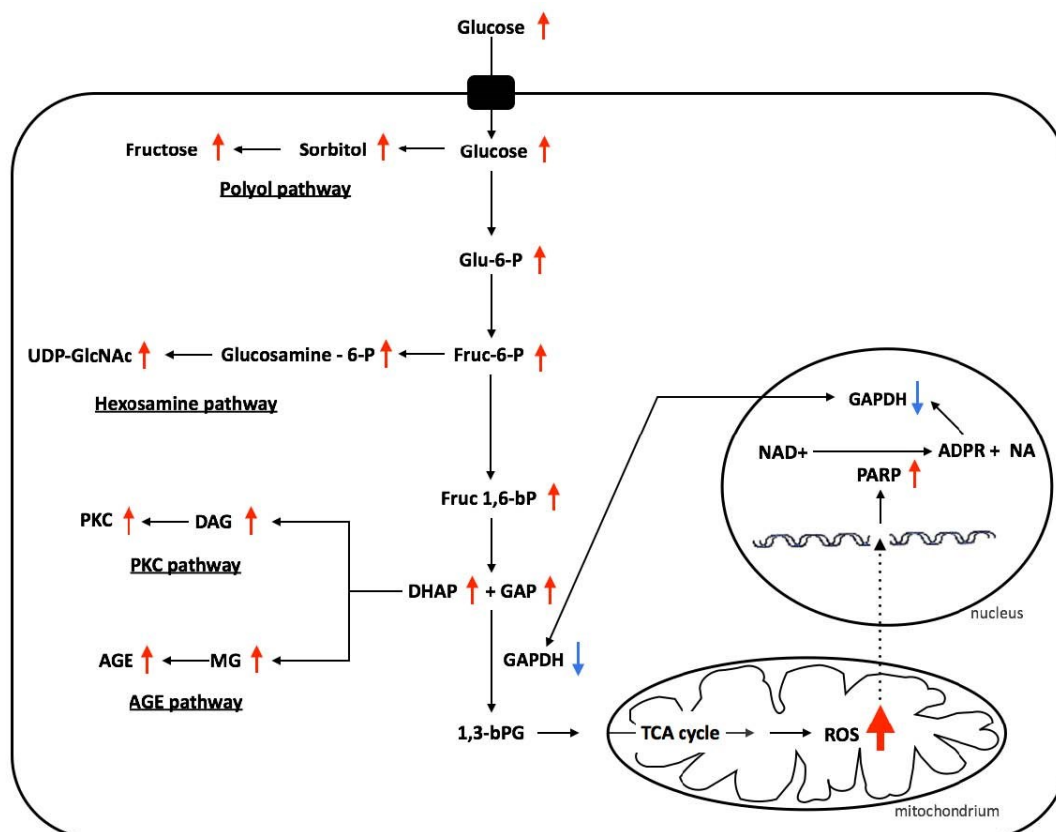
Figure 1. Scheme of the unifying theory. Adapted from (Brownlee, 2001).

GAPDH is an enzyme with multiple functions depending on its posttranslational modification and cellular localization (Nicholls et al., 2012; Tristan et al., 2011). The main function of the homo-tetrameric cytosolic GAPDH complex is the conversion of glyceraldehyde 3-phosphate (GAP) to 1,3-biphosphoglycerate (1,3-bPG). Several mechanisms for the transport of GAPDH in and out of the nucleus were reported including modifications such as acetylation and nitrosylation as well as Golgi apparatus mediated transport (Hara et al., 2005; Maruyama et al., 2002; Ventura et al., 2010). Once GAPDH is deactivated by poly-ADP-ribosylation, the conversion of GAP to 1,3-bPG is reduced, leading to an accumulation of glycolytic metabolites and

subsequently activation of the four major pathways of hyperglycemic damage (Du et al., 2003, 2000). Studies have demonstrated the inactivation of GAPDH under hyperglycemic conditions *in vitro* (Brownlee, 2005; Du et al., 2003, 2000). Moreover, studies in the retina of diabetic animals have shown a decrease in GAPDH activity in the progression of retinopathy (Kanwar and Kowluru, 2009; Madsen-Bouterse et al., 2010). The activity of GAPDH has been shown to be negatively correlated with plasma MG levels, which are increased in the progression of nephropathy (Beisswenger et al., 2005). However, it remains still unclear whether GAPDH is inactivated in the diabetic kidney.

The loss of GAPDH activity leads to a reduction in glycolysis and an accumulation of glucose and the metabolites of glycolysis within the cell. The elevated glucose levels are partially converted by aldose reductase into sorbitol, which is then oxidized to fructose (polyol pathway). Aldose reductase consumes NADPH, an essential cofactor for many reactions to detoxify ROS. The accumulation of sorbitol can result in hypertrophy and osmotic stress (Brownlee, 2005; Chung et al., 2003; Dagher et al., 2004; Lee and Chung, 1999).

As mentioned, the loss of GAPDH activity leads specifically to an accumulation in the metabolites up-stream of the triosephosphates (GAP and dihydroxyacetone phosphate, DHAP). The accumulation of these metabolites of glycolysis can be diverted into other pathways, for instance, fructose-6-phosphate (Fru-6-P) can be diverted into the hexosamine pathway. The end product of this pathway is uridine diphosphate N-actelyglucosamine, which is the substrate for posttranslational modifications of serine and threonine residues forming O-linked β-*N*-acetylglucosamine (O-GlcNAc). The O-GlcNAcylation results in changes in the expression of genes, which are associated with the development of diabetic complications such as TGF-β (Du et al., 2000; Schleicher and Weigert, 2000).

The accumulation of the triosephosphates can also lead to increased de novo synthesis of diacylglycerol (DAG), which enhances the activity of protein kinase C (PKC) (Xia et al., 1994). The PKC family consists of several isoforms. In diabetes PKC-α and PKC-β, which require DAG, Ca^{2+} and phospholipids, and PKC-δ and PKC-ε, which require only DAG, are elevated. The activation of PKC is linked to the development of

Introduction

late complications due to increase in extracellular matrix synthesis, angiogenesis or apoptosis (Geraldes and King, 2010).

Increased levels of triosephosphates can also result in the increased non-enzymatic formation of methylglyoxal (MG) by phosphate elimination (Phillips and Thornalley, 1993). MG is cytotoxic and preliminary detoxified by the glyoxalase system, which consists of glyoxalase I (GLO1) and glyoxalase II (GLO2) (Thornalley, 2003; Vander Jagt, 1993). In diabetes, increased formation of MG is associated with decreased activity of the glyoxalase system, and linked with the development of diabetic complications (Rabbani and Thornalley, 2011; Vander Jagt, 2008). If not detoxified, MG mainly reacts with arginine residues forming AGEs (Lo et al., 1994; Rabbani and Thornalley, 2012). Intracellular proteins, extracellular matrix proteins and circulating proteins can be glycated by MG to form AGEs. The formation of AGEs induces damage to the cell by: (1) changed gene transcription, (2) altered interaction between matrix components and receptors through the modification of extracellular proteins and (3) increased binding of glycated plasma proteins to the receptor for AGE (RAGE), leading to a proinflammatory response (Bierhaus et al., 2005; Brownlee, 2005; Lukic et al., 2008).

The described pathways are regarded to be activated under hyperglycemic conditions by ROS-induced inactivation of GAPDH in all organs which are affected by diabetic complications. Yet, the following questions remain unexplained in this theory:

1) Inactivation of GAPDH would lead to a decrease in the substrates of the TCA cycle resulting in decreased oxidative phosphorylation and diminished ROS production. Can the pathways of hyperglycemic damage be activated in diabetes despite this negative feedback mechanism?

2) Aldose reductase, the first and rate-limiting enzyme in the polyol pathway, has a low affinity to glucose (K_m of 100 mM) but diabetic endothelial cells have a glucose concentration of 30 nmol/mg protein (Bohren et al., 1992; Zhang et al., 2003). As such, it is debatable whether glucose can be considered as a substrate for aldose reductase *in vivo* or whether there are other mechanisms to activate the polyol pathway.

3) The studies underlying the unifying theory have been performed in different tissues and *in vitro* models. However, only few tissues have been examined for the activation of all pathways. Therefore, it remains unclear, whether all pathways are activated in every tissue, affected by hyperglycemia-induced damage.

2.3 How are ROS produced and how can they be detoxified?

Oxidative stress is defined as the imbalance between the production of ROS such as superoxide (O_2^-), hydrogen peroxide (H_2O_2) and hydroxyl radicals ($HO\bullet$) and the cellular capacity to detoxify these reactive intermediates. Under normal conditions ROS function as messengers in redox signaling and mildly increased ROS levels have been shown to have health-promoting effects (Ray et al., 2012; Ristow et al., 2009; Schmeisser et al., 2013). However, dramatically imbalanced ROS levels lead to the disruption of cellular signaling and increased cellular damage.

There are different sites of ROS production such as the mitochondria, endoplasmic reticulum, membranes and peroxisomes. ROS producing enzymes include the complexes involved in oxidative phosphorylation, NAD(P)H oxidase, xanthine oxidase and lipoxygenase (Aliciguzel et al., 2003; Guzik et al., 2002; Holmström and Finkel, 2014). According to the unifying theory, increased mitochondrial-derived ROS are central to the development of diabetic complications.

Within the body, 95 % of all inhaled O_2 undergoes a concerted four-electron reduction to produce water (Halliwell, 2006), (Figure 2). Although the ETC is an efficient system, side-reactions with molecular O_2 can occur resulting in its reduction to O_2^-. The primary sites for improper transfer of electrons are complex I and complex III of the ETC, however, the O_2^- production depends on the local concentrations of O_2 and electron donors such as NADH and $FADH_2$ (Murphy, 2009). On complex I two electrons are transferred in two one-electron steps to the freely diffusible electron carrier coenzyme Q (CoQ). It remains under debate which component of complex I is the major source of O_2^-. The NAD radical, semi-reduced CoQ, reduced flavin mononucleotice (FMN) as well as the iron-sulfur cluster are postulated to be involved in the production of O_2^- under physiological conditions

Introduction

(Kotlyar et al., 1990; Krishnamoorthy and Hinkle, 1988; Kudin, 2003; Kushnareva et al., 2002; Kussmaul and Hirst, 2006; Vinogradov and Grivennikova, 2005).
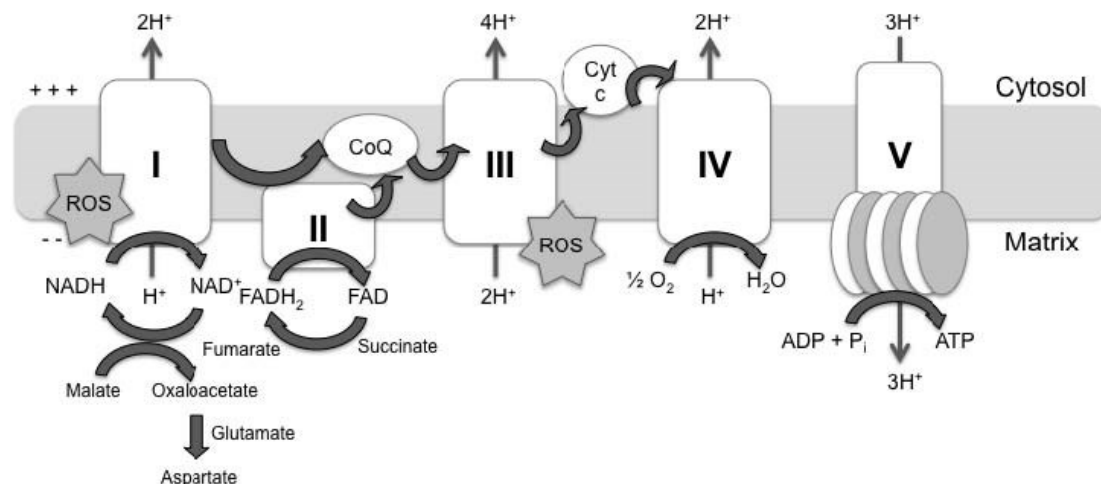
Figure 2. Scheme of the electron transport chain (ETC). Adapted from (Brownlee, 2001).

On complex III the electrons are transferred by asymmetric absorption and released within the Q-cycle from the two electron acceptor CoQ to the one electron acceptor cytochrome c (Mitchell, 1975). During this asymmetric absorption O_2^- can be generated. However, it remains under debate whether O_2^- is generated in a semiforward reaction directly by oxidation of an ubisemiquinone radical or in a semireverse reaction transmitted by oxidation of cytochrome b (Drose and Brandt, 2008; Gille and Nohl, 2001; Muller et al., 2002, 2004; Sarewicz et al., 2010).

Despite the short half-life (1 - 4 µs) and the limited sphere of influence of O_2^- (1 - 30 nm before it oxidizes a target), this and other ROS can target several cellular molecules such as proteins, lipids and DNA causing conformational changes, peroxidation, DNA crosslinks as well as strand breaks resulting in oxidative cell damage (Birben et al., 2012; Brand et al., 2004; Halliwell, 2006; Jena, 2012). To minimize the damaging effects of ROS, the body has evolved a number of multifaceted antioxidant defense systems which consist of low-molecular scavengers, such as glutathione and vitamins, as well enzymatic antioxidants. The major enzymatic antioxidants are superoxide dismutase (SOD) to detoxify O_2^-, catalase (CAT) to detoxify H_2O_2, glutathione peroxidase (GPX) to detoxify lipid peroxides and esterified peroxyl lipids (Chelikani et al., 2004; McCord and Fridovich, 1969; Mills, 1957).

2.4 Is glucose the right target to treat diabetic complications?

The unifying theory is based on studies which reported elevated ROS production under hyperglycemic conditions in *in vitro* systems. Subsequent studies reported increased oxidative stress also in diabetic patients. The Framingham study measured the oxidative stress marker 8-Epi-prostaglandin F2α in the urine and found a positive association between systemic oxidative stress and diabetes (Keaney, 2003). Oxidative stress, determined as 8-hydroxy-2-deoxy guanosine, was also increased in the glomeruli of diabetic patients with nephropathy (Jiang et al., 2010). H_2O_2 levels correlate positively to glycated hemoglobin (HbA_{1C}), an indicator of 3-month average plasma glucose, and negatively to uric acid, a systemic antioxidant, in the blood of patients with T1D (Francescato et al., 2014). However, with respect to the development of complications, plasma and intracellular markers of oxidative stress remain unchanged in the blood of T1D patients with and without complications (VanderJagt et al., 2001). In T2D, O_2^- production was increased in peripheral blood mononuclear cells and ROS production was found to be increased in lymphocytes of patients with nephropathy (Nam et al., 2008; Widlansky et al., 2010). The majority of these studies have only investigated ROS levels in the blood of diabetic patients and there have been no conclusive studies in human tissue to this date.

Hyperglycemia-mediated increase in ROS production and subsequent cellular changes are described as the main cause for the development of diabetic complications. As such, therapies have focused on the normalization of blood sugar and HbA_{1C}. These recommendations are mainly based on the results of the Diabetes Control and Complications Trail (DCCT) which consisted of 1441 patients with T1D. It was shown that only 11 % of late-complications in T1D patients can be explained by the duration of diabetes and the HbA_{1C} levels (DCCT Research Group, 1995). Lowering the HbA_{1C} levels, only reduced the absolute risk for albuminuria by 1.4 % with the NNT (number needed to treat) of 73.8 patients for 16 years and reduced the absolute risk of cardiovascular death by only 2.3 % in 30 years (DCCT/EDIC Research Group, 2011). The UKPDS study showed that lowering blood glucose in T2D had no effect on the development of cardiovascular complications and decreased the absolute risk for microvascular complications by only 2.4 % (UKPDS Study Group,

1998). Intensive therapy of T2D patients during the ACCORD study could not reduce the risk for microvascular outcomes and even increased mortality and was therefore stopped before the end of the study (Ismail-Beigi et al., 2010). In addition, it has been shown that the symptoms of diabetic neuropathy can be reduced after gastric bypass independent of glucose normalization (Müller-Stich et al., 2013). These studies show that the majority of diabetic patients do not benefit from lowering blood glucose levels with regard to the development of complications. Therefore, hyperglycemia cannot be considered as the only cause for diabetic complications. This is further reinforced by studies showing that diabetic complications can already develop before the clinical diagnosis of diabetes. In the United States more than 20 % of patients are already affected by retinopathy when they are diagnosed with diabetes and more than 24 % are affected by kidney disease (Harris et al., 1992; Plantinga et al., 2010).

2.5   Can experimental models help to understand diabetes?

The unifying theory describes glucose-induced increase in mitochondrial ROS production as the main cause for cellular damage leading to the development of diabetic complications. Oxidative stress is increased in the blood of T1D and T2D, however, only a small subset of patients benefit from intensive blood glucose lowering therapy. Many experimental studies have tried to analyze functional changes of the mitochondria in experimental models to clarify whether hyperglycemia affects mitochondrial ROS production and changes the antioxidative defense mechanism. The main experimental models to study diabetes are in mice and rats. Traditionally, T1D has been induced pharmacological in these models using β-cell toxins, such as streptozotocin (STZ) or alloxan. However, in the last decade, genetic models have been increasingly used which spontaneously develop diabetes due to genetic modifications, such as $Ins2^{+/-}$ Akita mice for T1D or db/db mice for T2D. It was shown that with respect to mitochondrial dysfunction in experimental diabetes, the results can vary considerably depending on the model, the type of diabetes, the organ studied and the methods used (Table 6 –10, Appendix).

Bugger et al. analyzed mitochondrial function such as ATP production and O_2 consumption in isolated mitochondria of different organs in type 1 diabetic

Introduction

Ins2$^{+/-}$ Akita mice (Bugger et al., 2009). In this study, ATP production remained unchanged in heart, liver and kidney. However, O$_2$ consumption was decreased in the cardiac mitochondria, unchanged in the hepatic mitochondria and increased in the renal mitochondria. In contrast, mitochondrial O$_2$ consumption of kidneys of STZ-induced Lewis rats remained unchanged after 8 weeks and decreased after 24 and 48 weeks of diabetes (Rosca et al., 2005). De Cavanagh et al. showed increased mitochondrial H$_2$O$_2$ production in isolated renal mitochondria of 12 week diabetic STZ-induced Sprague-Dawley rats (de Cavanagh et al., 2008). However, H$_2$O$_2$ production was decreased in renal mitochondria of wild type mice after 24 weeks of diabetes. Using the same model, O$_2^-$ production decreased *in vivo* when analyzed by real-time fluorescence imaging (Dugan et al., 2013). Besides the levels of oxidative stress, many studies analyzed the levels and activities of antioxidative enzymes, with contradictory findings. The activity of SOD1, the cytosolic form of the enzyme, was decreased in the heart of 8 week diabetic Wistar rats in one study but remained unchanged in the heart of 12 week diabetic Wistar rats in another (Aliciguzel et al., 2003; Godin et al., 1988). Kakkar et al. showed an increase in CAT activity in the liver of Sprague-Dawley rats, 1 week and 6 weeks after the induction of diabetes (Kakkar et al., 1998). Yet, using the same model Strother et al. showed decreased CAT after 4 weeks of diabetes (Strother et al., 2001). In the study of Aliciguzel et al. CAT activity was increased in the liver and kidney and decreased in the heart, however, in the study of Godin et al. CAT activity behaved oppositely in every tissue (Aliciguzel et al., 2003; Godin et al., 1988).

The contradictory results of these studies show that the results depend on the methods used as well as on the organ and model organism assessed. As such, these studies give no indication whether glucose-induced mitochondrial changes and subsequently increased ROS production are associated with the development of diabetic complication. Further studies are, therefore, required to clarify the following questions:

1) It is necessary to determine mitochondrial changes using the same techniques in all tissues of different diabetic models.

2) If changes of the mitochondria are observed, further studies will be required to determine whether glucose or other metabolites of glycolysis are responsible for the induction of mitochondrial changes. These studies are fundamental as intervention studies found only a minor association between blood glucose and the development of diabetic complications.

2.6   What is the aim of the study?

As shown, diabetes is a complex disease, which is still not completely understood and many studies point out that hyperglycemia cannot be considered as the only factor involved in the pathogenesis of diabetic complications (Nawroth et al., 2010).

The unifying theory, which is the predominant theory for the development of diabetic complications, is centered on glucose-induced increase in mitochondrial ROS production which leads to cellular damage. If this theory was correct, all complications would develop by the same mechanism and patients suffering from one complication would also be affected by the other complications. However, based upon the clinical evidence, diabetic patients tend to be more heterogeneous with respect to complications and different organs show distinct symptoms during the course of the disease. Thus, it needs to be analyzed whether the unifying theory can be applied to the development of all diabetic complications. Many studies have already analyzed changes in mitochondrial function in diabetes. However, as many different approaches have been used to assess mitochondrial function, the results have not been conclusive. Thus, this study was performed to determine the consistency of the effect of 3 months diabetes on the mitochondria in different tissues and 2 different mouse models (STZ and db/db), using standardized techniques. To assess different organs, the heart was chosen as a model for macrovascular complications, the kidney as a model for microvascular complications and the liver as an organ, which is classically not affected by diabetic complications.

Moreover, the activation of the four pathways of cellular dysfunction, as described by the unifying theory, were analyzed in the kidney as damage to this organ can be determined non-invasively by measurements of albumin secretion in the urine.

3 Material and Methods

3.1 Mouse models

Animal studies were approved by the Animal Care and Use Committee at the regional authority in Karlsruhe, Germany (file numbers: 35-9185.81/G-3/15, 35-9185.81/G-33/15, T-94/14). Male wild type mice (C57BL/6N) were obtained from Charles River, Sulzfeld, Germany. With about 3 months of age, diabetes type 1 was induced in wild type mice by intraperitoneal administration of streptozotocin (STZ, 60 mg/kg) for 5 consecutive days (Like and Rossini, 1976). Blood glucose was measured weekly using a glucometer and adjusted with insulin glargin (Lantus®, Sanofi) to <350 mg/dl. Male C57BL/6N-*Lepr*^{db} in the following only called db/db mice were kindly provided by the department of Cardiology, University Clinic Heidelberg. Db/db mice are homozygous for the diabetes mutation *Lepr*^{db} and develop type 2 diabetes at 4 weeks of age without the need for insulin treatment (Hummel et al., 1966). All mice were housed in groups with up to 4 animals in temperature- and humidity-controlled rooms (22°C, 55 %) with 12 h / 12 h light / dark cycle and given water and food ad libitum.

Mice were sacrificed by CO_2 inhalation and directly perfused through the heart via the vascular system using ice cold PBS. Heart, liver and kidney were dissected and either divided and flash-frozen in liquid nitrogen or used fresh for isolation of mitochondria.

3.2 Immunohistochemistry

Immunohistochemistry (IHC) was performed at the Institute of Pathology, Heidelberg. Tissue pieces (0.5 cm x 0.5 cm) were thawed and directly transferred into 4 % formalin and fixed at RT for 24 h. Fixed tissues were embedded into paraffin using the standard routine diagnostic protocol of the institute. Paraffin blocks were cut into 1 µm thick tissue sections using a HM 340E Rotary Microtome (Thermo Scientific Fisher) and mounted on glass microscope slides. Tissue sections were stained with hematoxylin and eosin (HE), Alcian blue/periodic acid–Schiff (AB-PAS) Masson's trichrome (trichrome) following routine diagnostic standard protocols of

the institute. Images were acquired with 20x magnification using a Hamamatsu NanoZoomer Digital Pathology system and analyzed using ObjectiveView™ 2.

3.3 Physiological parameters

All spectrophotometrical and flurometric assays were carried out using a BMG Labtech FLUOstar Omega multiplate reader.

3.3.1 Albumin secretion

Urine was collected for 4 h in metabolic cages and diluted 1:350. Albumin was determined using Mouse Albumin Elisa Kit, Immunology Consultants Laboratory and the protein concentration was determined using Bradford reagent (Bradford, 1976). Daily albumin secretion was calculated as µg albumin/24 h/g bodyweight.

3.3.2 Plasma cystatin C

Plasma samples were diluted 1:2,500 and cystatin C levels were determined using a commercially available Mouse Cystatin C Elisa Kit (RayBio®).

3.4 Mitochondrial function

3.4.1 Isolation of mitochondria

Mitochondria were isolated according to Cox and Emili with slight modifications (Cox and Emili, 2006). Briefly, tissue was homogenized in ice-cold isolation buffer I (250-STMDPS) containing 250 mM mannitol, 50 mM Tris (pH7.4), 5 mM $MgCl_2$, 1 mM DTT and 1 % protease inhibitor cocktail (P9599, Sigma) using a tight fitting teflon pestle. To isolate cardiac mitochondria 1 mg/ml collagenase IV was added to the extraction buffer. The lysate was centrifuged (800 g, 4 °C, 15 min, 3x). The supernatant served as a source for the mitochondria and was resuspended in isolation buffer II containing 280 mM mannitol, 10 mM $MgCl_2$, 5 mM K_2HPO_4, 10 mM MOPS, 1mM EGTA, pH 7.4 and centrifuged (6,000 g, 4°C, 15 min, 3x). Isolated mitochondria were resuspended in respiration buffer containing 250 mM sucrose, 15 mM KCl, 1 mM EGTA, 5 mM $MgCl_2$, 30 mM K_2HPO_4, pH 7.4 and protein concentration was determined using the Lowry protein assay (Lowry et al., 1951). Mitochondria were kept on ice and functional assays were performed within 4 h after isolation.

3.4.2 Purity of the mitochondria

Isolated mitochondria (100 µg) were stained with 300 nM MitoTracker® Green FM (M7514, ThermoFisher Scientific) in the dark at 37°C for 30 min. Subsequently, the mitochondria were washed 3 times and analyzed using a BD FACSCanto II system. The mitochondrial fraction showed a purity of more than 95 %.

3.4.3 ATP production

ATP production was determined using the ATPlite Luminescence Assay System (Perkin Elmer). Freshly isolated mitochondria were diluted in respiration buffer (see 4.3.1) and 0.5 µg isolated mitochondria, 12.5 mM malate, 12.5 mM glutamate and 1.65 mM ADP were added to a 96-well white microplate to measure state 3 respiration using malate, the substrate for complex I. State 3 respiration was also measured using succinate, the substrate for complex II. Therefore, 0.5 µg isolated mitochondria, 25 mM succinate and 1.65 mM ADP were added to a white microplate. After addition of the substrates, the plate was incubated for 8 min at 37°C on a heating plate. Meanwhile ATP standard 0.5 – 10 nmol were prepared in 100 µl respiration buffer and added to the plate. After incubation ATPlite Assay was performed by adding 50 µl of cell lysis buffer followed by 50 µl of substrate solution. The plate was shaken for 5 min and dark equilibrate for 5 – 10 min before the luminescence was measured.

3.4.4 Mitochondrial O_2 consumption

O_2 consumption was determined according to Will et al. using MitoXpress® Xtra, Luxcel Bioscience (Will et al., 2007). Freshly isolated mitochondria were diluted in respiration buffer (see 4.3.1). All reagents were warmed to 37°C and the microplate was prepared on a warming plate. To each well 100 µl MitoXpress probe reconstituted in 10 ml respiration buffer (see 3.4.1) and 50 µg isolated mitochondria, 12.5 mM malate, 12.5 mM glutamate and 1.65 mM ADP were added to a 96-well clear bottom black microplate to measure state 3 respiration using malate, the substrate for complex I. State 3 respiration was also measured using succinate, the substrate for complex II. Therefore, 25 µg isolated mitochondria, 25 mM succinate and 1.65 mM ADP were added to a clear bottom black microplate. Time-resolved

fluorescence (TRF) measurements were performed using a TRF reading head with a distance of 6 mm and applying 380 nm (excitation) and 655 nm (emission). The gain was set to 2,200 and the delay to 30 µs and 70 µs with of constant gate time of 30 µs. Data were processed according to Will et al. and the slope of the linear range was calculated.

3.4.5 O_2^- production

O_2^- production was measured using nitrotetrazolium blue chloride (NBT, Sigma-Aldrich), (Sim Choi et al., 2006). Freshly isolated mitochondria were diluted in respiration buffer and 15 µg were added in a 96-well clear microplate (see 4.3.1). 250 µl NBT in respiration buffer, 12.5 mM malate, 12.5 mM glutamate and 1.65 mM ADP were added to measure state 3 respiration using malate, the substrate for complex I. State 3 respiration was also measured using succinate, the substrate for complex II. Therefore, 25 mM succinate and 1.65 mM ADP were added to the mitochondria. The plate was incubated for 90 min at 37°C followed by a centrifugation step (4,000 rpm, RT, 5 min). The supernatant was discarded by inversion of the plate and applying a sharp flick of the wrist. The plate was gently tapped dry on paper towels and 200 µl of DMSO were added to dissolve the blue NBT formazan deposits. Absorbance spectrum (400 – 900 nm) was read and maximal absorbance was corrected for minimal absorbance.

3.4.6 H_2O_2 production

H_2O_2 production was measured using H_2DCFDA (Thermo Fisher Scientific). Freshly isolated mitochondria were diluted in respiration buffer and 2.5 µg mitochondria as well as 5 µM H_2DCFDA were added in a 96-well black microplate (see 4.3.1). To measure state 3 respiration with substrates for complex I and II, 12.5 mM malate, 12.5 mM glutamate and 1.65 mM ADP or 25 mM succinate and 1.65 mM ADP were added and the increase in fluorescence was measured over 30 min applying 485 +/- 12 nm (excitation), 520 nm (emission) and a gain of 1,500. The slope of the linear range was calculated as ΔRFU/min.

3.5 Enzymatic Assays

3.5.1 Protein isolation

Flash frozen tissue was grounded using an ice-cold mortar and 10 mg of tissue were resuspended in 200 µl of hypotonic buffer containing 50 mM K_2PO_4 and 10 mM $MgCl_2$ and sonicated twice with 10-15 % for 15 sec. Samples were then centrifuged (14,000 rpm, 4°C, 10 min) and the protein concentration of the supernatant was determined using the Bradford assay (Bradford, 1976). 0.5 - 8 µg tissue per well were used to determine CAT, GLO1, NQO1 and SOD activity in a 96-well plate format using a clear microplate unless otherwise indicated.

3.5.2 CAT activity

CAT activity was determined as the rate of disappearance by detecting the decrease in the absorbance of 240 nm using 0.036 % (w/w) H_2O_2 in 50 mM potassium phosphate buffer, pH 7.0 and an UV-transparent microplate (Beers and Sizer, 1952).

3.5.3 GLO1 activity

Glo1 activity was determined using the method described by Thornalley measuring the increase of absorbance at 240 nm and 37 °C due to S-D-lactoylglutathione formation from hemithioacetal generated by pre-incubation of MG and GSH at 37 °C for 10 min (Thornalley, 1988).

3.5.4 NQO1 activity

NQO1 activity was determined as the rate of increase in the absorbance of formazan at 650 nm. A reaction mixture containing glucose-6-phosphate and glucose-6-phosphate dehydrogenase continuously generated NADPH. This was used by NQO1 to reduce menadione which subsequently MTT to a blue formazan (Prochaska and Santamaria, 1988). To validate the measurement of NQO1 activity, the assay was also performed with 0.3 mM of the NQO1 inhibitor dicumarol (Sigma Aldrich) per well (He et al., 2006).

3.5.5   SOD activity

SOD activity was determined according to McCord and Fridovich by measuring the inhibition of the decrease in absorbance at 550 nm due to the reduction of cytochrome c (10 mM) by O_2^- radicals, which were produced by a coupled enzymatic reaction of xanthine oxidase (1.5 mU/ml) with atomar oxygen (McCord and Fridovich, 1969).

3.5.6   GAPDH activity

GAPDH activity was determined in cytosolic and nuclear extracts of kidney samples (see 3.7.2) measuring the increase in absorbance due to the reduction of NAD (Bergmeyer et al., 1974). 15 µg of protein were mixed with the reaction buffer containing 83 mM triethanolamine, 6.7 mM 3-phosphoglyceric acid, 3 mM L-cysteine, 2 mM $MgSO_4$, 0.1 mM NADH, 1.1 mM ATP and 3.3 U/ml 3 phosphoglyceric phosphokinase in a UV-transparent microplate and the increase in absorbance was measured at 340 nm for 10 min. To measure nuclear GAPDH activity 15 µg as well as 30 µg protein were used.

3.5.7   PKC activity

Flash frozen tissue was grounded using an ice-cold mortar and 10-20 mg of tissue were homogenized in PKC extraction buffer containing 25 mM Tris-HCl pH 7.4, 0.5 mM EDTA, 0.5 mM EGTA, 10 mM β-mercaptoethanol, 1 % protease inhibitor cocktail (P9599, Sigma). Samples were centrifuged (14,000 rpm, 4°C, 10 min) and the supernatant was transferred to a pre-equilibrated HiTrap™DEAD FF 1 ml column (GE Healthcare). The samples were washed with 5 ml PKC extraction buffer applying a flow rate of 1 ml/min. The samples were eluted using 5 ml PKC extraction buffer containing 200 mM NaCl, drop 32 – 58 were collected and the samples were stored at -80°C until analyzed. After thawing, the protein concentration of the eluate was determined using Bradford reagent (Bradford, 1976). The Activity was analyzed according to the manufacture's protocol (PKC kinase activity kit, Enzo Life Science) using 4.5 µg protein per well. Absorbance was measured at 450 nm and corrected for 570 nm.

3.6 Expression analysis

3.6.1 RNA extraction and cDNA synthesis

Flash frozen tissue was grounded using an ice-cold mortar and 10-20 mg of tissue were homogenized in RNA lysis buffer. The subsequent extraction was performed according to the manufactures protocol (PeqGold Total RNA Kit, Peqlab). Quantification of RNA was performed using a photometer (Eppendorf, GmbH). A total of 2 µg of RNA were used for the cDNA synthesis reaction and performed according to the manufactures protocol (High-capacity cDNA Reverse Transcription Kit, Thermo Fisher Scientific).

3.6.2 Quantitative real-time PCR

cDNA was diluted 1:6 with H_2O and used for qPCR analysis performed in duplicates with DyNAmo Flash SYBR Green qPCR Kit (Biozym). Briefly, 1 µl of cDNA was transferred into a 96-well qPCR microplate and 10 µl of reaction mix containing 1 x SYBR Green Mastermix, 200 nM forward primer and 200 nM reverse primer (Eurofins Genomics), (Table 8).

Table 1. Primer

Gene	Gene ID		Sequence [5' → 3']	Amplicon size, bps
B2m	12010	for	TTCTGGTGCTTGTCTCACTGA	104
		rev	CAGTATGTTCGGCTTCCCATTC	
Cat	12359	for	AGCGACCAGATGAAGCAGTG	181
		rev	TCCGCTCTCTGTCAAAGTGTG	
Glo1	109801	for	GATTTGGTCACATTGGGATTGC	110
		rev	TCCTTTCATTTTCCCGTCATCAG	
Gpx1	14775	for	AGTCCACCGTGTATGCCTTCT	105
		rev	GAGACGCGACATTCTCAATGA	
Gpx4	625249	for	GCCTGGATAAGTACAGGGGTT	99
		rev	CATGCAGATCGACTAGCTGAG	

Material and Methods

Gene	Gene ID		Sequence [5' → 3']	Amplicon size, bps
Hprt	15452	for	TCAGTCAACGGGGGACATAAA	142
		rev	GGGGCTGTACTGCTTAACCAG	
Nqo1	18104	for	AGGATGGGAGGTACTCGAATC	144
		rev	AGGCGTCCTTCCTTATATGCTA	
Nrf2	18024	for	TCTTGGAGTAAGTCGAGAAGTGT	140
		rev	GTTGAAACTGAGCGAAAAAGGC	
Polr2b	231329	for	GACGACGATGAGATCACTCCG	152
		rev	GGTGCATCTTCCACAATTCTTTG	
Rn18s	19791	for	CGGCTACCACATCCAAGGAA	187
		rev	GCTGGAATTACCGCGGCT	
Sod1	20655	for	AACCAGTTGTGTTGTCAGGAC	139
		rev	CCACCATGTTTCTTAGAGTGAGG	
Sod2	20656	for	CAGACCTGCCTTACGACTATGG	113
		rev	CTCGGTGGCGTTGAGATTGTT	
Tbp	21374	for	AGAACAATCCAGACTAGCAGCA	120
		rev	GGGAACTTCACATCACAGCTC	
Ywhaz	22631	for	GAAAAGTTCTTGATCCCCAATGC	134
		rev	TGTGACTGGTCCACAATTCCTT	

The plate was sealed with a film and centrifuged (1000 rpm, 4°C, 1 min). Quantitative real-time PCR analysis was performed using Roche Lightcycler 480 applying the following protocol (Table 9).

The cross-points (Cp) were calculated and the relative ratio of the mRNA levels were determined applying the following formula $2 \times (2^{Cp(target)-Cp(reference)})^{-1}$ and using the geometric mean of the Cp values of *B2m, Hprt, Polr2b, Rn18s, Tbp, Ywhaz* as a reference (Hruz et al., 2011; Svingen et al., 2015).

Table 2. Thermocycler protocol for qPCR

Step	Temperature, °C	Time	Ramp rate, °C/sec	Number of cycles
Pre-incubation	95	7 min	4.4	1
Amplification	95	10 sec	4.4	45
	60	20 sec	2.2	
	72	1 sec	4.4	
Melting curve	95	5 sec	4.4	1
	65	1 min	2.2	
	97	5 acquisitions per °C	0.11	
Cooling	4	forever	4.4	1

3.7 Immunoblotting

3.7.1 Whole tissue protein extracts

For whole tissue lysis, flash frozen tissue was grounded using an ice-cold mortar and 10 – 20 mg grounded tissue were resuspended with a syringe in RIPA buffer containing 50mM Tris-HCl pH 7.5, 150 mM NaCl, 1 % Triton X-100, 0.5 % Na-deoxycholate, 0.1 % SDS, 1 mM DTT, 1 % protease inhibitor (P9599, Sigma) and 40 U/ml benzonase (Millipore). The samples were incubated on ice for 1 h with periodic vortexing and centrifuged (14,000 rpm, 4°C, 30 min). Protein concentration of the supernatant was determined using Bradford reagent and the samples were stored at -20°C until used (Bradford, 1976).

3.7.2 Cytoplasmic and nuclear protein extracts

Flash frozen tissue was grounded using an ice-cold mortar and 20 mg grounded tissue were resuspended in lysis buffer containing 10 mM HEPES pH 7.9, 1.5 mM MgCl$_2$, 10 mM KCl, 0.5 mM DTT, 0.05 % NP40 and 1 % protease inhibitor cocktail (P9599, Sigma). The samples were vortexed, incubated on ice for 10 min and subsequently centrifuged (3,000 rpm, 10 min, 4°C). The supernatant containing the cytoplasmic fraction was transferred to a new tube and the pellet was washed with lysis buffer until clear, before resuspending it in nuclear buffer containing 5 mM

HEPES pH 7.9, 1.5 mM MgCl$_2$, 500 mM NaCl, 0.2 mM EDTA, 0.5 mM DTT, 26 % glycerol and 1 % protease inhibitor cocktail. The samples were vortexed, incubated on ice for 20 min and sonicated at 10-15 % power for 10 sec twice. The samples were centrifuged (14,000 rpm, 4°C, 10 min) and the supernatant containing the nuclear fraction was transferred to a new tube. Protein concentration of cytoplasmic and nuclear fraction was determined using Bradford reagent (Bradford, 1976).

3.7.3 Immunoblotting

About 10-30 µg protein were mixed with Laemmli buffer containing 0.8 % SDS, 4 % glycerol, 100 mM DTT, 25 mM Tris-HCl pH 6.8, 0.005 % bromophenol blue and cooked at 95°C for 10 min (Laemmli, 1970). Proteins were resolved by SDS-PAGE (4-15 % Mini-PROTEAN TGX, Biorad) applying 180 V for 45 min and transferred onto a nitrocellulose membrane applying 25 V for 27 min. Transfer was checked using Ponceau Red and membranes were blocked using 2 % milk powder in PBS-T or in the case of O-GlcNAc with Pierce Protein-Free Blocking Buffer (Thermo Scientific Fisher). After 1 h blocking at RT, the primary antibody was added in the appropriate concentration (Table 10). After overnight incubation at 4°C the blots were washed with PBS-T and incubated with the secondary antibodies coupled to horseradish peroxidase (Table 11) for 1 h at RT. The proteins were detected using ECL reagent (GE Healthcare). For reprobing, membranes were stripped in a 80°C water bath for 20 min using 0.2 M glycine pH 2.5 and 0.05 % Tween 20. Afterwards the membranes were washed with PBS-T, blocked and processed as mentioned above. Images were acquired and quantified using the GS-800™ calibrated densitometer and Quantity One ® 1-D analysis software, Bio-Rad.

Table 3. Primary antibodies

Antibody for	Isotype	Company	Dilution
CAT	Rabbit	14097, Cell Signaling Technology	1: 3,000
GAPDH	Rabbit	181602, abcam	1: 10,000
GLO1	Rat	81461, abcam	1: 1,500
Histone H3	Rabbit	4499, Cell Signaling Technology	1: 3,000

Antibody for	Isotype	Company	Dilution
NQO1	Mouse	28947, abcam	1:3,000
O-GlcNAc	Mouse	677902, Biolegend	1: 1,000
PKC-α	Mouse	8393, Santa Cruz Biotechnology	1:500
PKC-δ	Rabbit	937, Santa Cruz Biotechnology	1:500
SOD1	Mouse	20926, abcam	1: 1,500
SOD2	Rabbit	13533, abcam	1:5,000

As the common cytosolic loading controls β-actin and GAPDH were increased in the kidney of both diabetic models, the nuclear specific loading control histone H3 was used for whole tissue protein extracts.

Table 4. Secondary antibodies

Antibody for	Company	Dilution
Mouse	7076, Cell Signaling Technology	twice the dilution of the first antibody
Rabbit	7074, Cell Signaling Technology	
Rat	7077, Cell Signaling Technology	

3.8 Metabolomics

3.8.1 Determination of adenosine compound levels

Adenosine compounds were extracted from freshly grounded renal tissue (15-25 mg) with 0.25 ml ice-cold 0.1 M HCl in an ultrasonic ice-bath for 10 min. The resulting homogenates were centrifuged (16,400 g, 4°C, 10 min) to remove cell debris. Adenosines were derivatized with chloroacetaldehyde as previously described and separated by reversed phase chromatography on an Acquity BEH C18 column (150 mm x 2.1 mm, 1.7 µm, Waters) connected to an Acquity H-class UPLC system (Bürstenbinder et al., 2007). Prior separation, the column was heated to 42°C and equilibrated with 5 column volumes of buffer A (5.7 mM TBAS, 30.5 mM KH_2PO_4 pH 5.8) at a flow rate of 0.45 ml/min. Separation of adenosine derivates was achieved by increasing the concentration of buffer B (2/3 acetonitrile in 1/3 buffer A) in buffer A as follows: 1 min 1 % B, 1.6 min 2 % B, 3 min 4.5 % B, 3.7 min 11 % B,

10min 50 % B, and return to 1 % B in 2 min. The separated derivates were detected by fluorescence (Acquity FLR detector, Waters, excitation: 280 nm, emission: 410 nm) and quantified using ultrapure standards (Sigma). Data acquisition and processing was performed with the Empower3 software suite (Waters).

Adenosine compound levels were kindly quantified by Dr. Gernot Poschet at the Centre for Organismal Studies (COS), University Heidelberg.

3.8.2 Determination of organic acid and sugar levels

Organic acids and sugars were extracted of 15-25 mg grounded tissue using 400 µl ultra-pure water and heated at 95°C for 20 min. Organic acids were separated using an IonPac AS11-HC (2mm, ThermoScientific) column connected to an ICS-5000 system (ThermoScientific) and quantified by conductivity detection after cation suppression (ASRS-300 2mm, suppressor current 95-120 mA). Prior separation, the column was heated to 30°C and equilibrated with 5 column volumes of solvent A (ultra-pure water) at a flow rate of 0.38 ml/min. Separation of anions and organic acids was achieved by increasing the concentration of solvent B (100mM NaOH) in buffer A as follows: 8 min 4 % B, 18 min 18 % B, 25 min 19 % B, 43 min 30 % B, 53 min 62 % B, 53.1 min 80 % B for 6 min, and return to 4 % B in 11 min. Soluble sugars were separated on a CarboPac PA1 column (ThermoScientific) connected to the ICS-5000 system and quantified by pulsed amperometric detection (HPAEC-PAD). Column temperature was kept constant at 25°C and equilibrated with 5 column volumes of solvent A (ultra-pure water) at a flow rate of 1 ml/min. Baseline separation of carbohydrates was achieved by increasing the concentration of solvent B (300mM NaOH) in solvent A as follows: From 0 to 25 min 7.4 % B, followed by a gradient to 100 % B within 12 min, hold for 8 min at 100 % B, return to 7.4 % B and equilibration of the column for 12 min. Data acquisition and quantification was performed with Chromeleon 7 (ThermoScientific) (Neubert et al., 2016).

Organic acid and sugar levels were quantified by Dr. Gernot Poschet at the Centre for Organismal Studies (COS), University Heidelberg.

3.8.3   Determination of MG levels

The concentration of MG was determined by stable isotope dilution analysis liquid chromatography with tandem mass spectrometric detection (LCMSMS), as described previously (Rabbani and Thornalley, 2014). Briefly, 10 mg of tissue were deproteinized by addition of 10 μl of 20 % trichloroacetic acid. The internal standard, 2 pmol of $[^{13}C_2]$-MG (prepared in-house), were added and MG derivatized by incubation with 100 μM 1,2-diamonbenzene, 100 μM diethylenetriaminepenta-acetic acid, 5 mM sodium dithionite stabilizer and 0.3 % (w/v) NaN_3 in the dark at RT for 4 h (Dobler et al., 2006; Thornalley and Rabbani, 2014). Samples were assayed by LC-MS/MS using an ACQUITY UPLC-I class with a Xevo TQ-S mass spectrometric detector, Water Cooperation. Samples were separated using a BEH C18 column (ACQUITY, 1.7 μm, 100 x 2.1 mm, Waters Corporation) fitted with a pre-column (ACQUITY, 1.7 μm, 5 x 2.1 mm, Waters Corporation). The mobile phase was 0.1 % formic acid with a linear gradient of 0-100 % of 0.1 % formic acid in 50 % (v/v) acetonitrile over 10 min at a flow rate of 0.2 ml/min. The column was washed with 100 % of 0.1 % formic acid in 50 % (v/v) acetonitrile and re-equilibrated with 100 % of 0.1 % formic acid. The analysts were detected by positive ionization with multiple reaction monitoring with a retention time of 5.9 min. Mass transition (parent ion > fragment ion; collision energy; cone voltage) were: MG 145.01 > 77.10; 24 eV; 2 V & $[^{13}C_2]$-MG 148.06 > 77.16; 24 eV; 2 V. Other mass spectrometer settings were: capillary voltage 0.5 kV, source temperature 150 °C, desolvation gas temperature 350 °C, desolvation gas flow 800 l/h and cone gas flow 150 l/h. A calibration curve was constructed from 0-20 pmol of MG. The limit of detection was 0.520 pmol.

3.9   Statistical analysis

All statistical analyses were performed in GraphPad Prism 7 and the level for statistical significance was defined as $p < 0.05$. Outlier elimination was performed applying Tuckey's method of leveraging the interquartile range (Tukey, 1977). The function of the mitochondria was assessed using one control and one diabetic mouse per day. To minimize day-to-day variation, mitochondrial function was analyzed separately for each day. The mean of the control measurements for each day was normalized to 1 and the diabetic measurements were calculated as an

arithmetical ratio to the respective control. Differences between data groups of mitochondrial function were evaluated for significance using one-sample t-test. Significance of all other measurements was calculated using unpaired t-test assuming Gaussian distribution.

4 Results

4.1 Tissue specific changes in the function of the mitochondria of type 1 and type 2 diabetic mice

4.1.1 Physiological characterization of the experimental models

Type 1 and type 2 diabetic mouse models on the C57BL/6N background were analyzed for diabetes-induced functional changes of the mitochondria. T1D was induced to male wild type mice (C57BL/6N) by intraperitoneal administration of the β-cell toxin STZ at about 3 months of age. Blood glucose levels were increased in the diabetic mice (BL6-STZ) compared to the age-matched, non-diabetic littermates (BL6-ctrl) and weekly adjusted with insulin to < 350 mg/dl. On the day of sacrifice the plasma glucose levels were determined as 188 +/- 43 mg/dl for the BL6-ctrl mice vs 402 +/- 130 mg/dl for the BL6-STZ mice, p < 0.001 (Table 5). T2D was studied in db/db mice on the C57BL/6N background, which were homozygous for the diabetes mutation $Lepr^{db}$, and age-matched non-diabetic littermates (db/m). The db/db animals developed diabetes spontaneously at about 4 weeks without the need for insulin treatment. On the day of sacrifice the plasma glucose levels were determined as 169 +/- 20 mg/dl for the db/m mice vs 300 +/- 29 mg/dl for the db/db mice, p < 0.001 (Table 5). After induction of diabetes the BL6-STZ mice stopped increasing weight resulting in a decreased bodyweight compared to the controls (35.7 +/- 2.5 g vs 23.8 +/- 3.0 g, p < 0.001). In contrast, the db/db mice gained more weight than their respective controls (24.8 +/- 1.6 vs 47.6 +/- 1.5 g, p < 0.001). The differences in bodyweight were also reflected in changed wet weights of several tissues; the heart of the BL6-STZ mice showed a decreased wet weight (0.13 vs 0.18 g, p < 0.001) and the liver of the db/db mice showed an increased wet weight when compared to the controls (1.6 +/- 0.3 vs 4.8 +/- 1.2 g, p < 0.001). IHC stainings of the liver showed local cellular infiltration in the BL6-STZ mice indicating mild inflammation (Figure 3, blue arrow). IHC stainings of the enlarged liver of the db/db mice showed an accumulation of fat droplets indicating hepatic steatosis (Figure 3, yellow arrow), which was not accompanied by inflammation or fibrosis as assessed by HE, AB-PAS and trichrome stainings (Figure 3).

Results

Table 5. Basic and physiological parameters of the experimental animals

Nomenclature	Type 1 diabetes			Type 2 diabetes		
	control	diabetic		control	diabetic	
	BL6-ctrl	BL6-STZ		db/m	db/db	
Age of animals, d	203 +/- 13			130 +/- 16		
Duration of diabetes, d	0	121 +/- 29		0	110 +/- 16	
Plasma glucose, mg/dl	188 +/- 43	402 +/- 130	***	169 +/-20	300 +/- 29	***
Bodyweight (BW), g	35.7 +/- 2.5	23.8 +/- 3.0	***	24.8 +/- 1.6	47.6 +/- 1.5	***
Wet weight of heart, g	0.18 +/- 0.0	0.13 +/- 0.0	***	0.13 +/- 0.0	0.14 +/- 0.0	
Wet weight of liver, g	1.7 +/- 0.3	1.6 +/- 0.4		1.6 +/- 0.3	4.8+/- 1.2	***
Wet weight of kidney, g	0.54 +/- 0.0	0.58 +/- 0.1		0.44 +/- 0.1	0.43 +/- 0.1	
Albumin in urine, µg/24 h/g BW	0.4 +/- 0.4	1.4 +/- 0.5	***	0.7 +/- 0.5	1.9 +/- 0.6	*
Plasma cystatin C, µg/ml	5.4 +/- 0.6	4.5 +/- 0.6	*	5.1 +/- 0.7	5.4 +/- 0.6	

Data are expressed as mean +/- SD. For type 1 and type 2 diabetic study groups n = 10 and 9, respectively. For statistical analysis two sided t-test was applied * $p < 0.05$ and *** $p < 0.001$ vs non-diabetic control.

Results
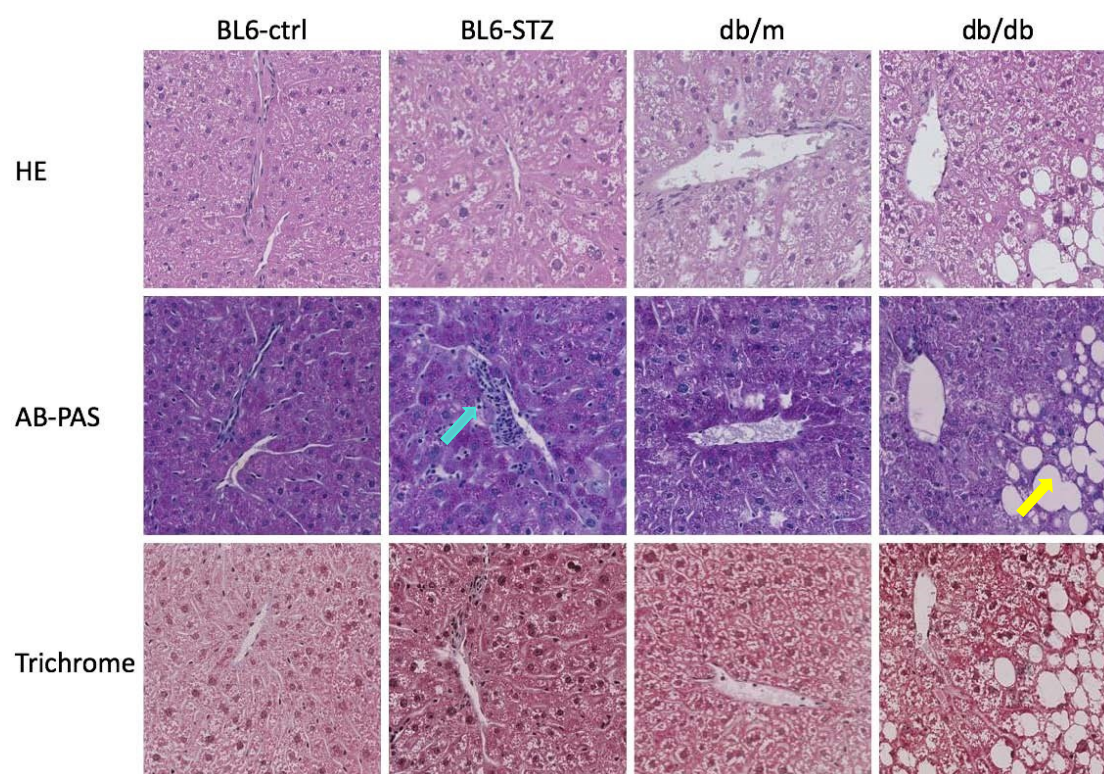
Figure 3. IHC stainings of the liver: inflammation and steatosis in the diabetic liver

Representative photomicrographs of liver sections are shown. Of each experimental group 3 livers were stained with hematoxylin and eosin (HE), Alcian blue/periodic acid–Schiff (AB-PAS) and (Masson's) trichrome. The blue arrow indicates cellular infiltration and the yellow arrow indicates fat droplets. Original magnification x20.

IHC stainings were performed in the kidney and glomeruli, showing vas afferens and efferens, were assessed. The Bowman's capsule of the control mice was filled with parietal epithelial cells (Figure 4, orange arrow), however, the cells within the capsule were missing in the BL6-STZ mice, leaving an empty space within the Bowman's capsule (Figure 4, green arrow). Besides, the basement membrane of the glomeruli was thickened in the BL6-STZ mice (Figure 4, AB-PAS). Changes in the structure of the glomeruli affected the function of the kidney, which was assessed by increased albumin output in the urine (0.4 +/- 0.4 vs 1.4 +/- 0.5 µg/ 24 h/ g BW, p < 0.001) and hyperfiltration indicated by decreased plasma cystatin C levels (5.4 +/- 0.6 vs 4.5 +/- 0.6 µg/ml, p < 0.05), (Table 5). In the kidney of the db/db mice, loss of epithelial cells, increase in space of the Bowman's capsule and thickening of the basement membrane were not present. Despite unchanged morphology of the glomeruli, the function of the kidney changed as shown by increased albumin secretion (0.7 +/- 0.5 vs 1.9 +/- 0.6 µg/ 24 h/ g BW, p < 0.05), however, without

changes in plasma cystatin C levels (Table 5). These results suggest that both diabetic mouse models were affected by early stages of nephropathy.
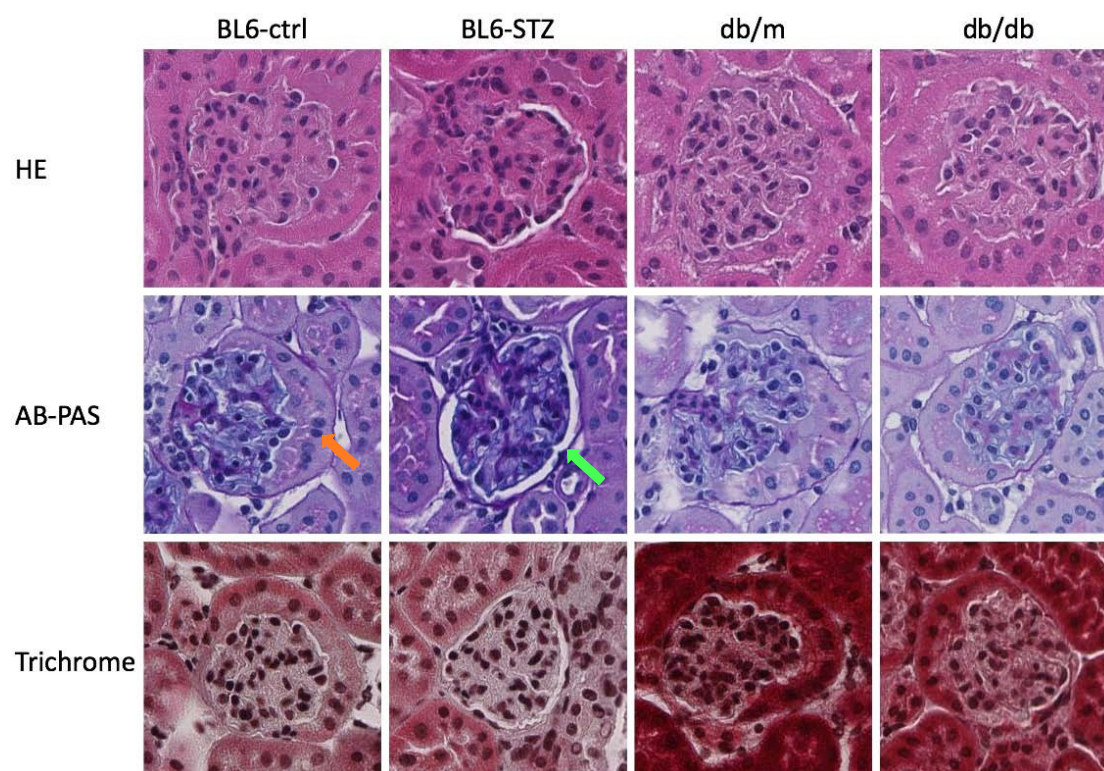
Figure 4. IHC stainings of the kidney: basement membrane thickening and loss of epithelial cells in T1D

Representative photomicrographs of one glomerulus with vas afferens und efferens. Of each experimental group 3 kidneys were stained with hematoxylin and eosin (HE), Alcian blue/periodic acid–Schiff (AB-PAS) and (Masson's) trichrome. Orange arrow indicates parietal epithelial cells. Green arrow indicates thickening of basement membrane and increase in space of the Bowman's capsule. Original magnification x20.

Due to the limited amount of material, no IHC staining of the heart was performed.

4.1.2   Intracellular metabolite concentrations

Despite an increase in plasma glucose (Table 5), intracellular glucose levels were decreased in the liver of the BL6-STZ mice (31.9 +/- 7.7 vs 24.9 +/- 5.3 nmol/mg tissue, p < 0.05) and remained unchanged in the liver of the db/db mice (Figure 5). Unlike in the liver, glucose concentrations were increased in the kidney of both diabetic models (type 1: 1.0 +/- 0.3 vs 19.3 +/- 0.7 nmol/mg tissue, p < 0.001, type 2: 0.8 +/- 0.3 vs 3.6 +/- 0.3 nmol/mg tissue, p < 0.001). In the liver of the BL6-STZ mice the concentration of malate and succinate, substrates of the TCA cycle, remained unchanged. However, in the liver of the db/db mice the levels of malate

decreased (1.0 +/- 0.2 vs 0.4 +/- 0.1 nmol/mg tissue, $p < 0.001$) and the levels of succinate showed a tendency to increase (0.09 + /- 0.01 vs 0.29 +/- 0.18 nmol/mg tissue, $p = 0.06$). In the kidney the levels of malate did not change in any of the models. The levels of succinate were unchanged in the kidney of the BL6-STZ model but showed a tendency to decrease in the db/db model (0.4 +/- 0.2 vs 0.2 +/- 0 nmol/mg tissue, $p = 0.07$).

Intracellular glucose

Intracellular malate

Intracelluar succinate
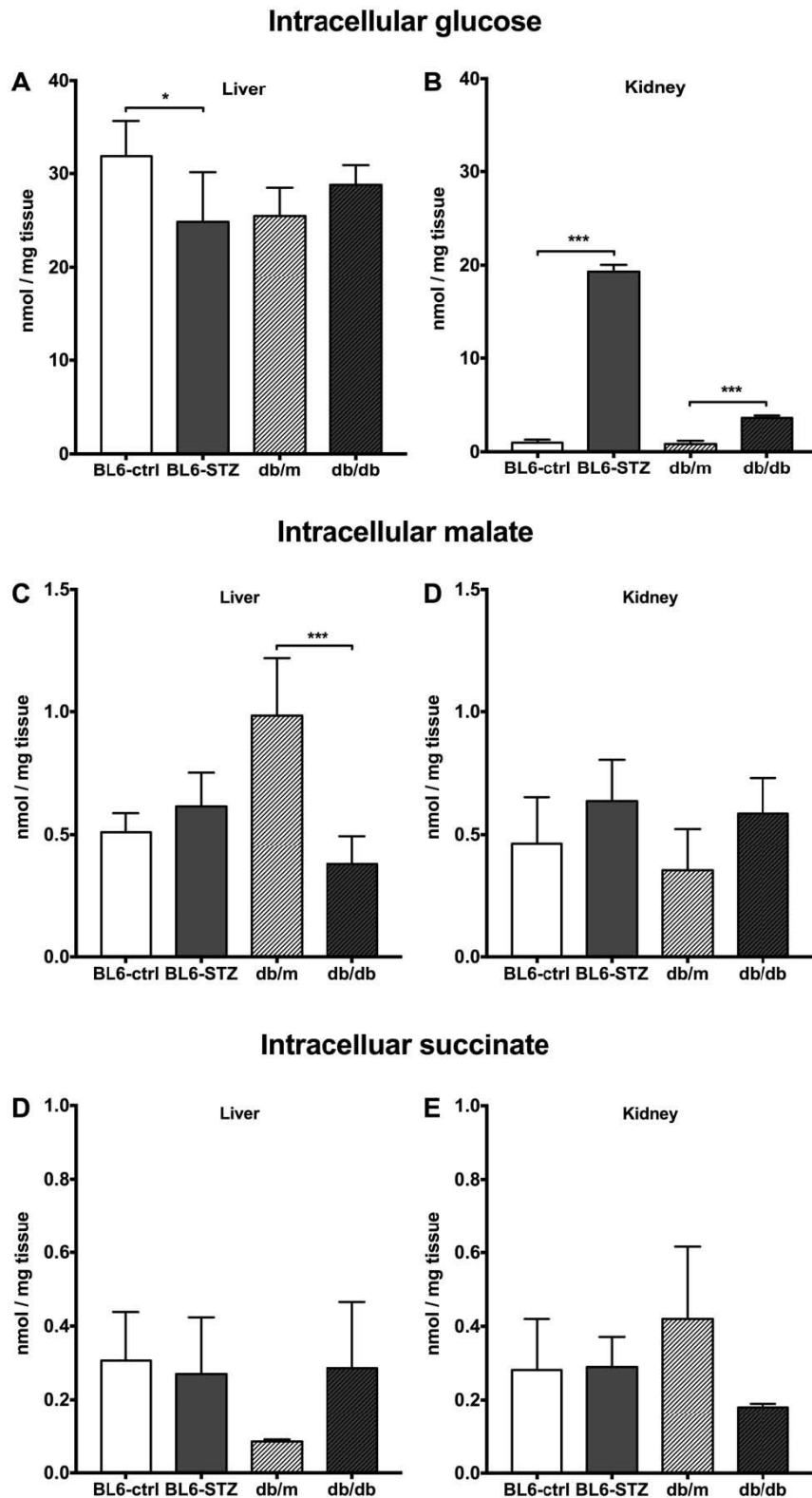
Figure 5. Changes in intracellular metabolite concentrations in liver and kidney

(A/B) Intracellular glucose, **(C/D)** malate and **(E/F)** succinate concentrations were quantified by liquid chromatography. For type 1 and type 2 diabetic study groups n = 6 and 5, respectively. Data is expressed as mean +/- SD. For statistical analysis two sided t-test was applied * p < 0.05 and *** p < 0.001 vs non-diabetic control.

Results

4.1.3 Mitochondrial function

Mitochondrial ATP production, in response to the complex I substrate malate, did not change in the heart of the BL6-STZ or the db/db mice when compared to the respective controls, which were set to 1 (Figure 6.A). In the liver, ATP production did not change in the BL6-STZ mice but showed a tendency to increase in the db/db mice (1.7 +/- 0.7 fold change, p = 0.1), (Figure 6.B). Renal mitochondria of both models did not show changes in ATP production (Figure 6.C).

Mitochondrial ATP production, in response to the complex II substrate succinate, was unchanged in the heart of the BL6-STZ mice and decreased in the db/db mice (0.7 +/- 0.2 fold change, p < 0.05), (Figure 6.D). In the liver, ATP production did not change in the BL6-STZ mice but showed a tendency to increase in the db/db mice (2.0 +/- 0.9 fold change, p = 0.07), (Figure 6.E). Renal mitochondria of the BL6-STZ mice showed increased ATP production (1.3 +/- 0.1 fold change, p < 0.05) whereas ATP production remained unchanged in the db/db mice (Figure 6.F).
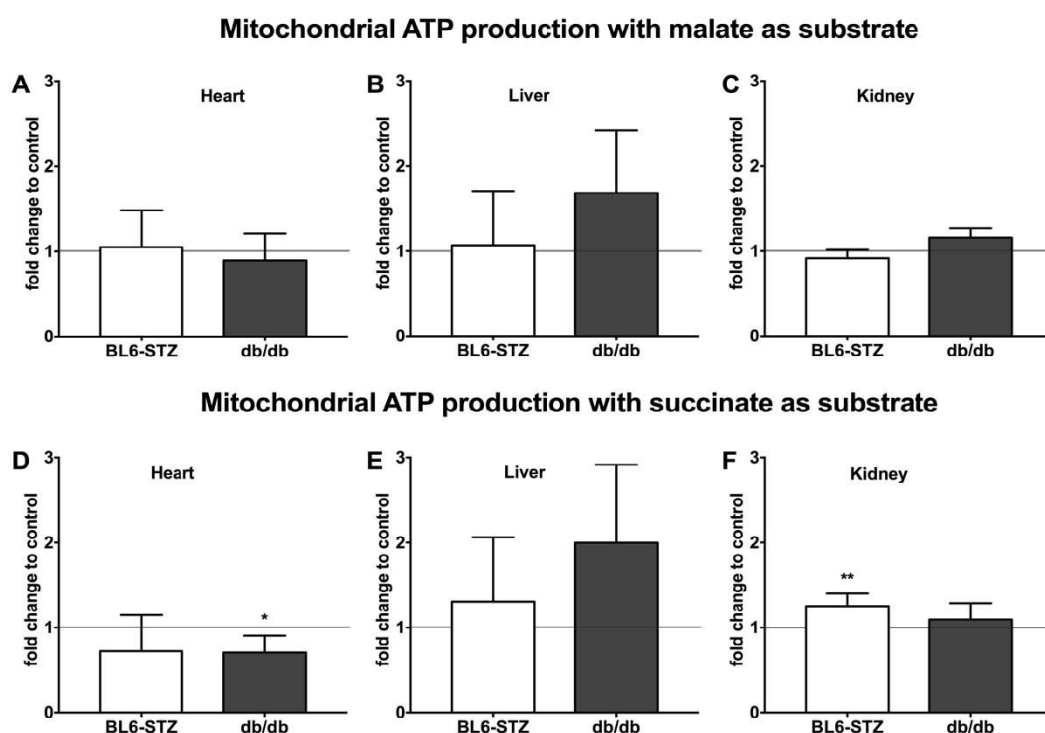
Figure 6. ATP production in isolated mitochondria of heart, liver and kidney

ATP production was measured with a luminescent assay in **(A)** heart, **(B)** liver and **(C)** kidney using malate, glutamate and ADP as substrates for complex I. Using succinate and ADP as substrates for complex II ATP production was measured in **(D)** heart, **(E)** liver and **(F)** kidney. For type 1 and type 2 diabetic study groups n = 10 or 5. Data is expressed as mean +/- SD. For statistical analysis the non-diabetic controls were set 1 and one sample *t*-test was applied * p < 0.05.

In the liver, the AMP level did not change in the BL6-STZ mice but decreased in the db/db mice (654 +/- 92 vs 475 +/- 50 pmol/mg tissue, p < 0.01), (Figure 7.A). ADP and ATP levels as well as energy charge did not change in the liver of any model (Figure 7.C, E, G). In the kidney of the BL6-STZ mice, AMP levels showed a tendency to increase (474 +/- 129 vs 658 +/- 260 pmol/mg tissue, p < 0.15), but no change in AMP levels were observed in the kidney of the db/db mice (Figure 7.B). ADP levels showed a tendency to decrease in the kidney of the BL6-STZ mice (344 +/- 151 vs 202 +/-11 pmol/mg tissue, p < 0.1) but remained unchanged in the db/db mice (Figure 8.D). ATP levels showed a tendency to decrease in the BL6-STZ mice (138 +/- 79 vs 77 +/- 47 pmol/mg, p < 0.15) but remained unchanged in the db/db mice (Figure 7.F). Despite trends of changed nucleotide levels, the overall energy charge was unchanged in both models (Figure 7.H). This suggests, that the mitochondria change their function and adapt to the diabetic conditions and thus preserve the cellular energy homeostasis.
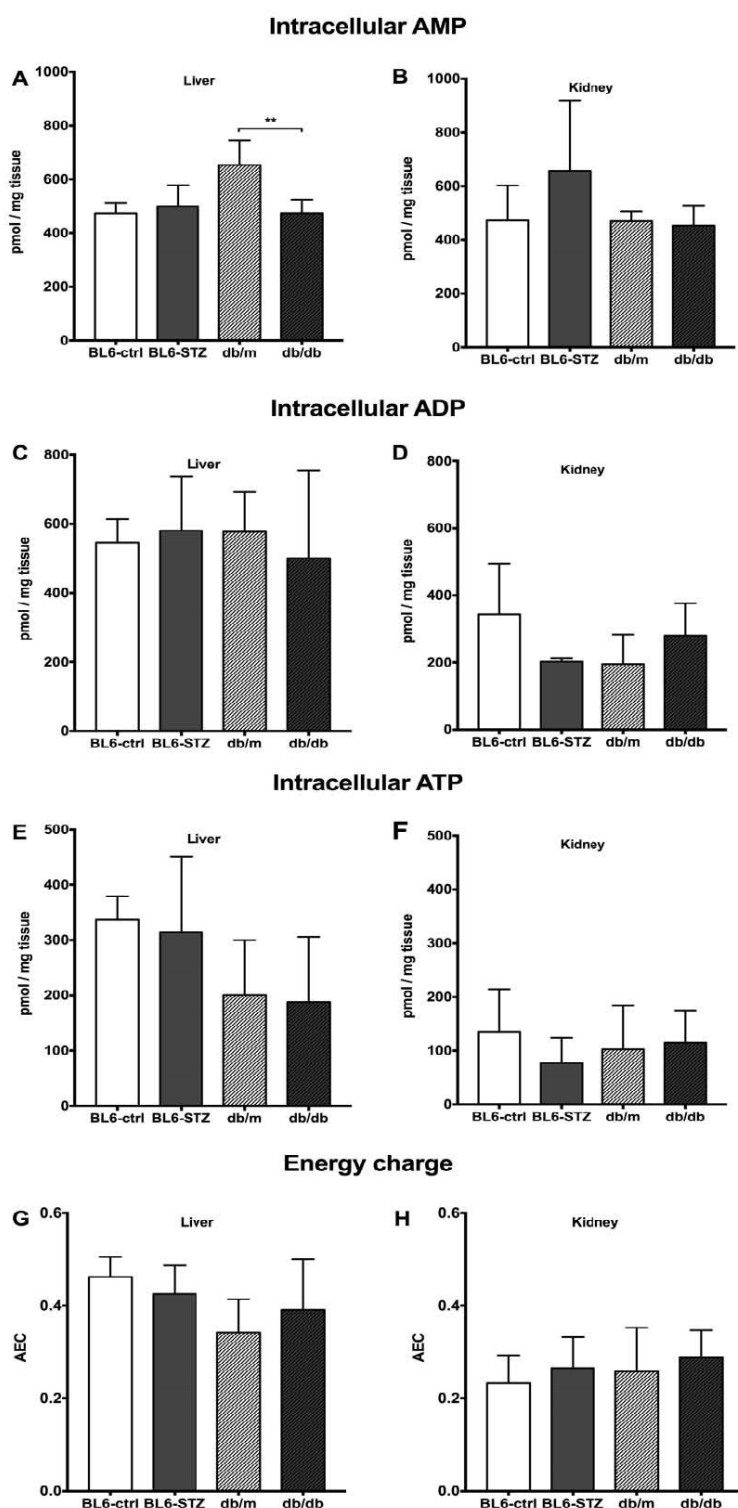
Figure 7. Changes in intracellular metabolite concentration in liver and kidney

(A/B) AMP, **(C/D)** ADP and **(E/F)** ATP concentrations were quantified by liquid chromatography coupled fluorescence detection. **(G,H)** Energy charge was calculated applying the following formula: $([ATP] + 0.5 \, [ADP]) \times ([ATP] + [ADP] + [AMP])^{-1}$. For type 1 and type 2 diabetic groups n = 6 and 5, respectively. Data is expressed as mean +/- SD. For statistical analysis two sided *t*-test was used. ** p < 0.01 vs non-diabetic control.

Results

Mitochondrial function was analyzed with respect to O_2 consumption. Using malate as substrate for complex I, O_2 consumption was unchanged in the heart, liver and kidney of both diabetic models (Figure 8.A-C).

Using succinate as substrate for complex II, O_2 consumption was decreased in the heart of the BL6-STZ mice (0.06 +/- 0.04 fold change, $p < 0.001$) as well as in the db/db mice (0.68 +/- 0.07 fold change, $p < 0.01$), (Figure 8.D). In the liver, O_2 consumption showed a tendency to increase in the BL6-STZ mice (4.4 +/- 1.7 fold change, $p = 0.07$) and was increased in the db/db mice (10.3 +/- 5.4 fold change, $p < 0.05$), (Figure 8.E). In the kidney of the BL6-STZ mice, O_2 consumption remained unchanged whereas it was decreased in the db/db mice (0.3 +/- 0.2 fold change, $p < 0.001$), (Figure 8.D).
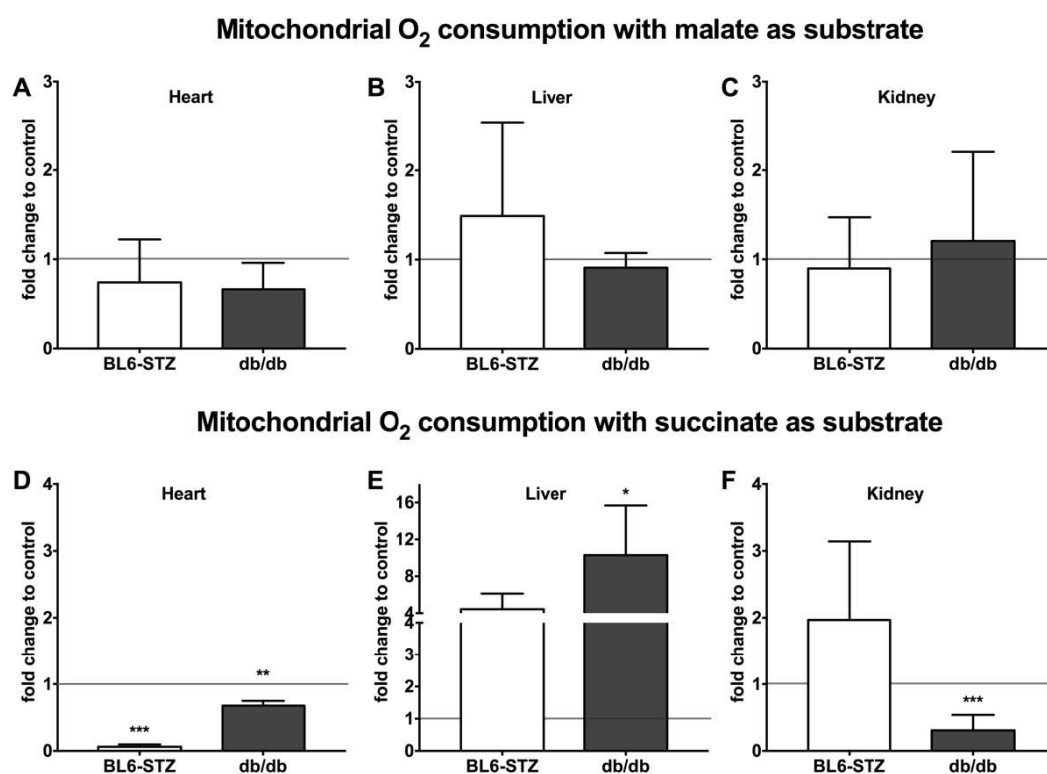
Figure 8. O_2 consumption in isolated mitochondria of heart, liver and kidney

O_2 consumption was measured with a fluorescent assay in **(A)** heart, **(B)** liver and **(C)** kidney using malate, glutamate and ADP as substrates for complex I. Using succinate and ADP as substrates for complex oxygen consumption was measured in **(D)** heart, **(E)** liver and **(F)** kidney. For type 1 and type 2 diabetic study groups n = 10 and 5, respectively. Data is expressed as mean +/- SD. For statistical analysis the non-diabetic controls were set 1 and one sample t-test was applied * $p < 0.05$, ** $p < 0.01$, *** $p < 0.001$.

Results

The majority of the differences between control and diabetic mice with regard to ATP production and O_2 consumption were observed using succinate as a substrate for the ETC, suggesting that the function of complex II was altered in the mitochondria of diabetic animals. Moreover, it has been shown that the effect of diabetes on the function of the mitochondria was organ- and model-dependent.

4.1.4 Mitochondrial ROS production

Using the complex I substrate malate, O_2^- production did not change in cardiac mitochondria of the BL6-STZ mice. However, O_2^- production was decreased in cardiac mitochondria of the db/db mice (0.87 +/- 0.02 fold change, $p < 0.01$), (Figure 9.A). In the liver and kidney of both models O_2^- production did not change (Figure 9.B + C).
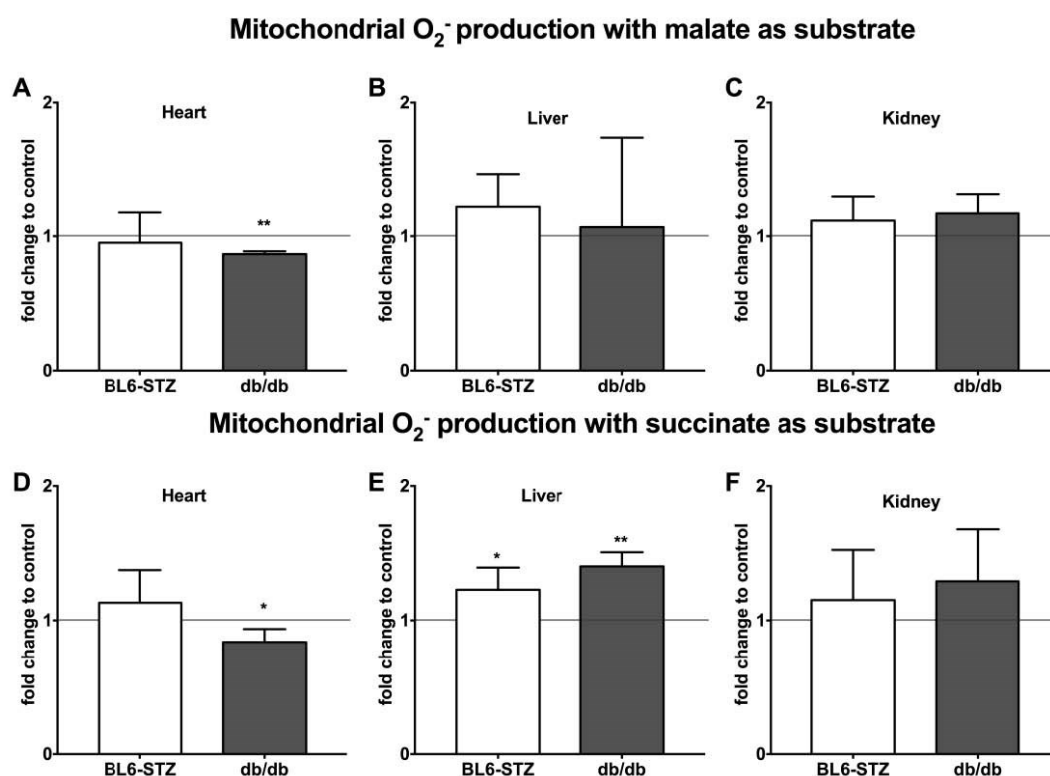
Figure 9. Production of O_2^- in isolated mitochondria of heart, liver and kidney

O_2^- was quantified as NBT-diformazan formation in isolated mitochondria of **(A)** heart, **(B)** liver and **(C)** kidney using malate, glutamate and ADP as substrates for complex I. Using succinate and ADP as substrates for complex II ATP production was measured in **(D)** heart, **(E)** liver and **(F)** kidney. For type 1 and type 2 diabetic study groups n = 6 and 5, respectively. Data is expressed as mean +/- SD. For statistical analysis the non-diabetic controls were set 1 and one sample *t*-test was applied * $p < 0.05$, ** $p < 0.01$.

Results

Using the complex II substrate succinate, O_2^- production did not change in the cardiac mitochondria of the BL6-STZ mice but decreased in the db/db mice (0.8 +/- 0.1 fold change, $p < 0.05$), (Figure 9.D). Regarding the liver, O_2^- production was slightly increased in the BL6-STZ mice (1.2 +/- 0.2 fold change, $p < 0.05$) as well as in the db/db mice (1.4 +/- 0.1 fold change, $p < 0.01$), (Figure 9.E). O_2^- production remained unchanged in isolated mitochondria of the kidney of both models when compared to their respective controls.

The production of H_2O_2 was analyzed to rule out the possibility that the excess in O_2^- was detoxified by SOD. Using malate as a substrate, H_2O_2 production did not change in the heart of any of the analyzed models (Figure 10.A). H_2O_2 production was also not changed in the liver of the BL6-STZ mice but increased in the db/db mice (1.5 +/- 0.1 fold change, $p < 0.01$), (Figure 10.B).

Mitochondrial H_2O_2 production with malate as substrate

Mitochondrial H_2O_2 production with succinate as substrate
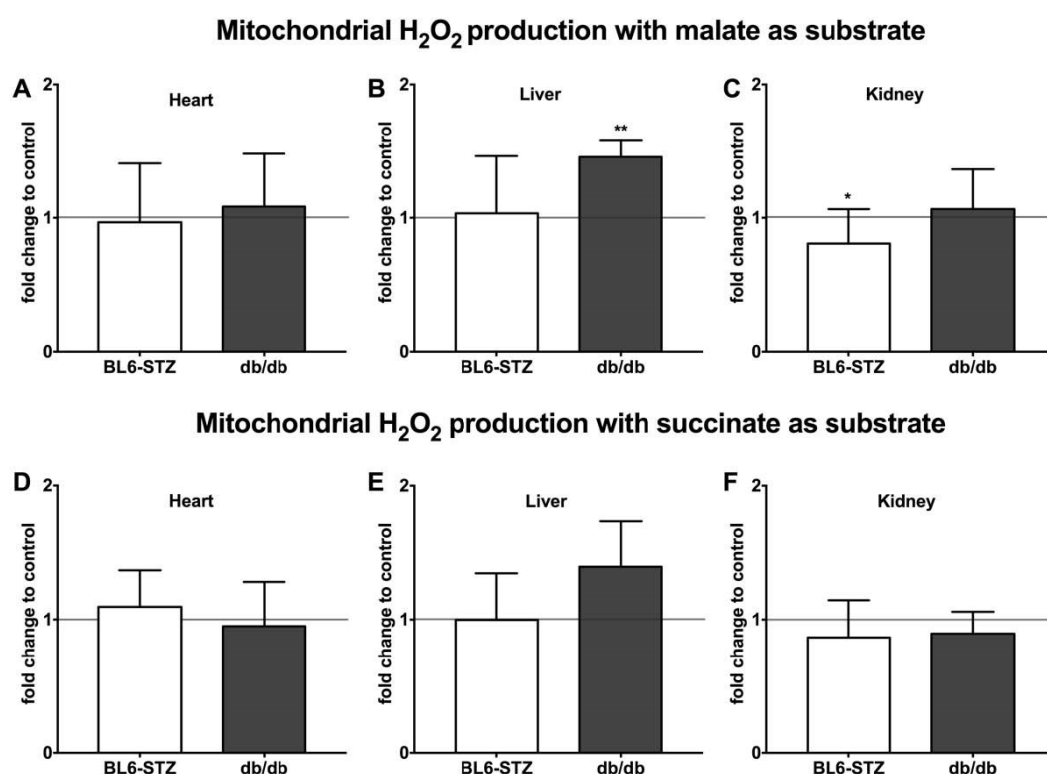
Figure 10. Production of H_2O_2 in isolated mitochondria of heart, liver and kidney

H_2O_2-induced increase in fluorescent intensity of H_2-DCF was measured in isolated mitochondria of **(A)** heart, **(B)** liver and **(C)** kidney using malate, glutamate and ADP as substrates for complex I. Using succinate and ADP as substrates for complex II H_2O_2 production was measured in **(D)** heart, **(E)** liver and **(F)** kidney. For type 1 and type 2 diabetic study groups n = 10 and 5, respectively. Data is expressed as mean +/- SD. For statistical analysis the non-diabetic controls were set 1 and one sample t-test was applied ** $p < 0.01$.

Results

In the kidney, H_2O_2 production decreased in the BL6-STZ mice (0.81 +/- 0.26 fold change, $p < 0.05$) but remained unchanged in the db/db mice. Using succinate, H_2O_2 production remained unchanged in the heart of both models (Figure 10.D). In the liver, H_2O_2 production did not change in the BL6-STZ mice but showed a tendency to increase in the db/db mice (1.4 +/- 0.3 fold change, $p = 0.06$), (Figure 10.E). In the kidney of both models H_2O_2 production remained unchanged (Figure 10.F).

4.2 Is there a ROS-independent activation of the pathways of hyperglycemic damage in early nephropathy?

Diabetes-induced changes of mitochondrial function and ROS production were found to be not only model, but also tissue dependent. In general, the changes observed were not associated with each other, i.e. increased mitochondrial function was not associated with increased ROS production, which is in contradiction to the unifying theory. This lack of association was particularly evident in the kidney, which despite having increased albumin secretion, an indication of the early stages of nephropathy, as well as increased intracellular glucose, showed increased mitochondrial function but no increased ROS production. Further analysis, with respect to the antioxidant defenses, as well as activation of the four pathways of cellular dysfunction, as described by the unifying theory, was therefore performed in the kidney.

4.2.1 The antioxidant defense mechanisms were not increased

The mRNA levels of the cytosolic enzyme to detoxify O_2^-, *Sod1* decreased in the BL6-STZ mice (1 +/- 0.2 vs 0.6 +/- 0.3 fold change, $p < 0.05$) but remained unchanged in the db/db mice. The mRNA expression levels of all other antioxidant genes including *Sod2*, *Cat*, *Gpx1* and *Gpx4* did not change in any of the mouse models (Figure 11.A). The change in *Sod1* mRNA level was not reflected in the protein level, which remained unchanged in the BL6-STZ mice, however, SOD1 protein level decreased in the db/db mice (1 +/- 0.3 vs 0.3 +/- 0.2 fold change, $p < 0.5$) despite unchanged mRNA levels (Figure 11.B + C). Protein levels of SOD2, the isoform located in the mitochondria, remained unchanged in both models and was associated with unchanged total SOD activity (Figure 11.B, D + E).

Results

As H_2O_2 production was unchanged or decreased in the kidney, protein levels and activity of the H_2O_2 detoxifying enzyme CAT were also analyzed. CAT protein levels were decreased in the BL6-STZ mice (1 +/- 0.1 vs 0.4 +/- 0.1 fold change, p < 0.01) and the db/db mice (1 +/- 0.1 vs 0.7 +/- 0 fold change, p < 0.01), (Figure 11.B + F). Assessing activity, the decrease in CAT protein levels was only reflected in the db/db mice (1 +/- 0.1 vs 0.7 +/- 0.1 fold change, p < 0.01) but not in the BL6-STZ mice (1 +/- 0.3 vs 0.9 +/- 0.1 fold change), (Figure 11.G).
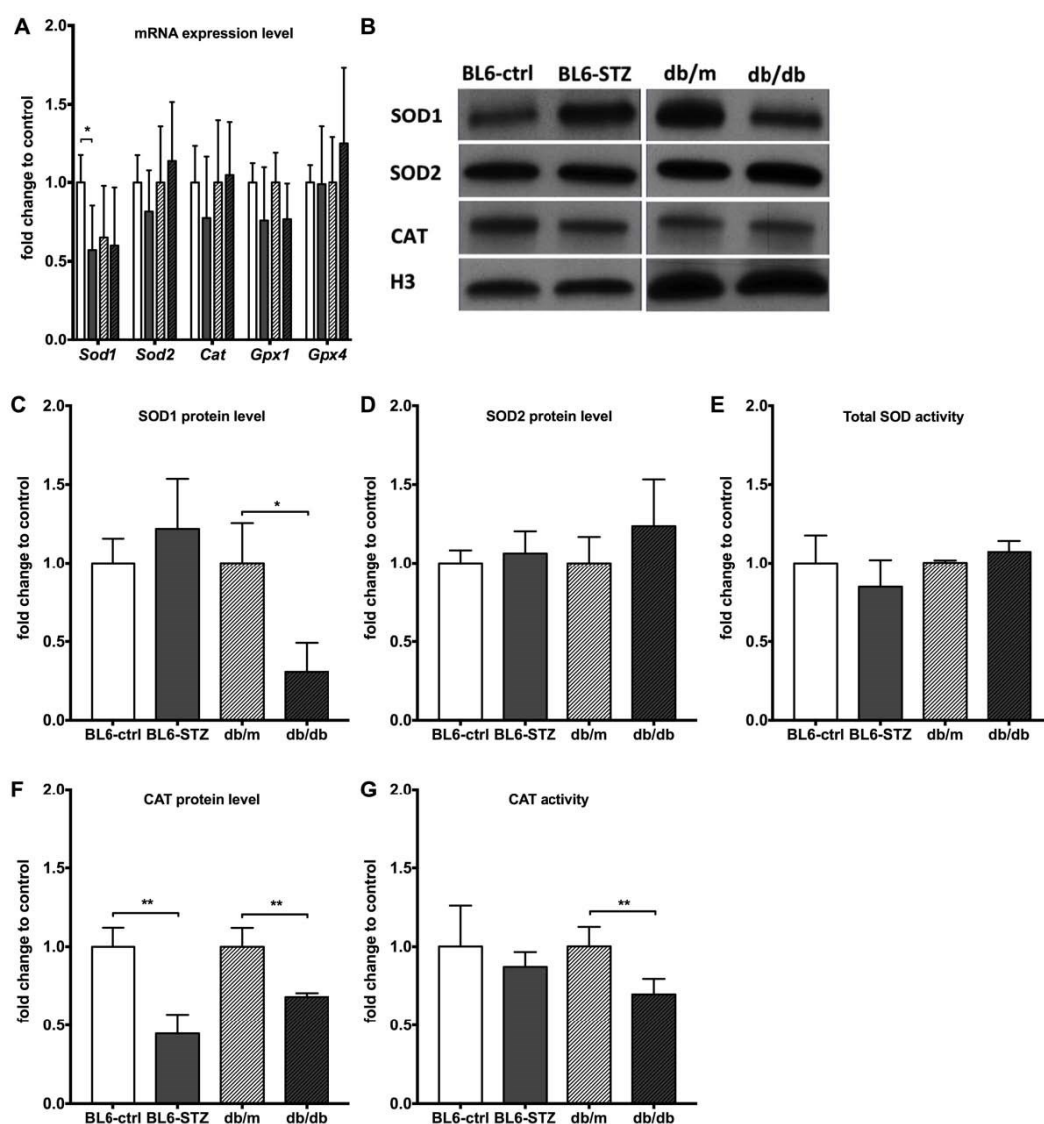
Figure 11. Analysis of the antioxidant status in the kidney of type 1 and type 2 diabetic mouse models

(A) Gene expression **(B, D, E)** SOD1 and SOD2 protein levels and total activities **(C, D, F)** CAT protein level and activity were measured using qPCR, WB analysis and spetrophotometrical assays. H3 of one representative WB is shown. For type 1 and type 2 diabetic study groups n = 8 or 4 (mRNA), n = 4 (protein) and n = 5 or 4 (activity). Data is expressed as mean +/- SD. For statistical analysis two sided *t*-test was applied * p < 0.05, ** p < 0.01 vs non-diabetic control.

Results

As the activity of antioxidant enzymes has been shown to correlate negatively with the production of ROS, it can be concluded, that the production of O_2^- was unchanged in both models. Unchanged CAT activity suggests that the H_2O_2 levels remained unchanged in the kidney of the BL6-STZ mice. However, H_2O_2 production seems to be increased in the db/db mice as the CAT activity was decreased in this model.

4.2.2 GAPDH was not inactivated

GAPDH protein levels increased in the cytosol of renal cells in the BL6-STZ mice (1 +/- 0.8 vs 9.3 +/- 5.7 fold change, $p < 0.05$) and in the db/db mice (1 +/- 0.4 vs 2.7 +/- 0.2 fold change, $p < 0.01$), (Figure 12.A-D). However, the total activity of cytosolic GAPDH remained unchanged (Figure 12.E). Regarding nuclear GAPDH, neither protein nor activity could be detected in the nuclear fraction (Figure 12.C + D).
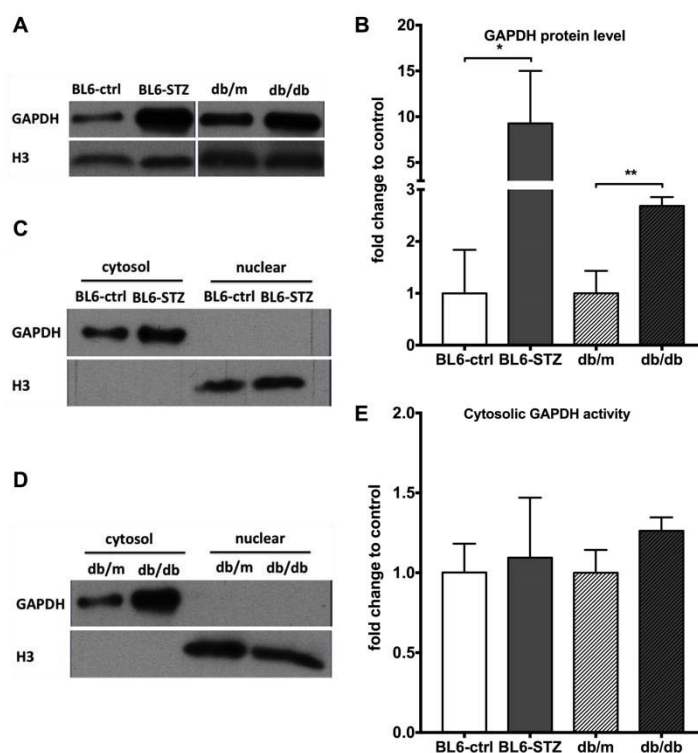
Figure 12. Cytosolic and nuclear distribution and activity of GAPDH in the kidney of type 1 and type 2 diabetic mouse models

(A, B) GAPDH protein level in total lysate as well as in **(C,D)** cytosolic and nuclear fraction in **(C)** BL6-STZ and **(D)** db/db mice were determined using WB analysis. **(E)** GAPDH activity was measured in the cytosolic fraction using a spectro-photometrical assay. Nuclear activity could not be determined. For type 1 and type 2 diabetic study groups n = 4 (protein) and n = 5 or 4 (activity). Data is expressed as mean +/- SD. For statistical analysis two sided t-test was applied * $p < 0.05$, ** $p < 0.01$ vs non-diabetic control.

4.2.3 The PKC pathway was not activated

The protein levels of PKC-α and PKC-δ did not change in the total cell extract of the BL6-STZ mice (Figure 13.A-C). These unchanged protein levels were reflected in unchanged total PKC activity in the cytosol of the BL6-STZ mice (Figure 14.D). In the db/db model, however, PKC-α levels decreased (1 +/- 0.1 vs 0.4 +/- 0.4 fold change, $p < 0.05$) whereas PKC-δ levels increased (1 +/- 0.3 vs 1.7 +/- 0.3 fold change, $p < 0.05$) in the total cell extract (Figure 13.A–C). These uneven changes were accompanied by unchanged total PKC activity in the cytosol (Figure 13.D).
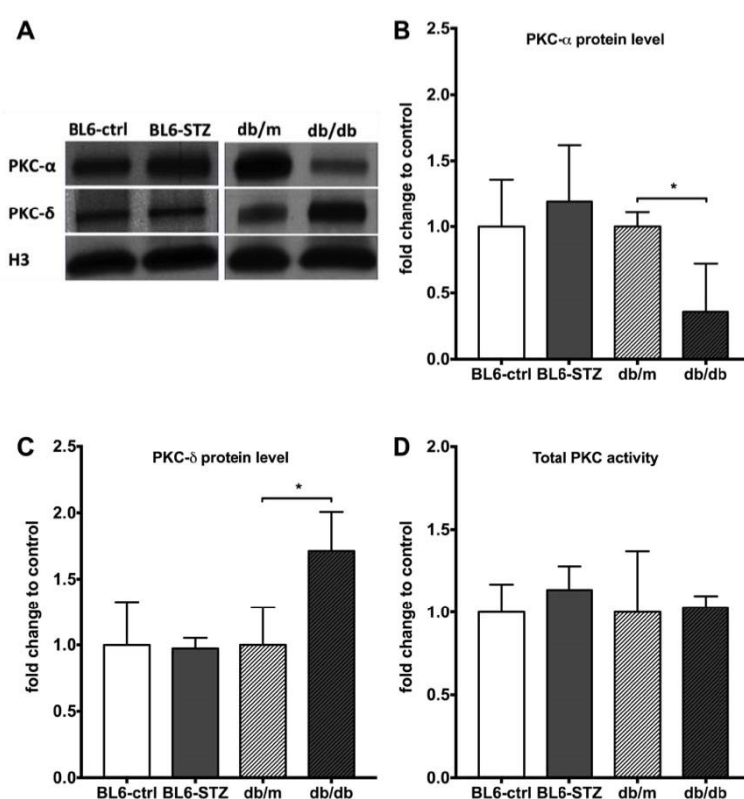
Figure 13. PKC expression and activity in the kidney of type 1 and type 2 diabetic mice

(A, B, C) PKC-α and PKC-δ protein levels were determined using WB analysis. For better visualization (not for analysis) of PKC-δ, background was subtracted in the BL6-ctrl and the BL6-STZ mice. H3 of one representative WB is shown. **(D)** Total PKC activity was measured using an ELISA utilizing a synthetic peptide as a substrate for PKC. For type 1 and type 2 diabetic study groups n = 4 (protein) and n = 5 or 4 (activity). Data is expressed as mean +/- SD. For statistical analysis two sided *t*-test was applied * $p < 0.05$ vs non-diabetic control.

4.2.4   The production of the AGE precursor MG was not increased

MG showed a tendency to increase in the BL6-STZ mice (474 +/- 129 vs 658 +/- 260 pmol / mg tissue, p = 0.15) but remained unchanged in the db/db mice (Figure 14.A). Increased MG formation is accompanied by decreased activity of the glyoxalase system (Rabbani and Thornalley, 2011; Vander Jagt, 2008). Therefore, changes regarding Glo1, the first enzyme of MG detoxification, were further assessed. Glo1 mRNA and protein levels as well as the activity were not increased in any of the diabetic models (Figure 14.B–E).
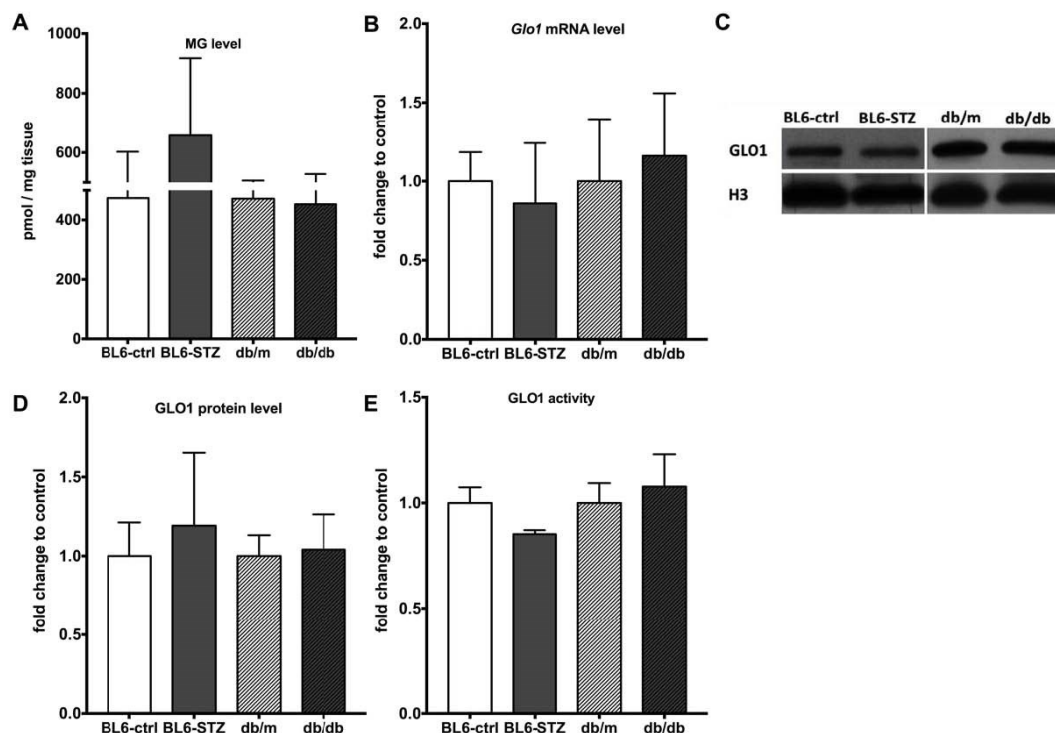
Figure 14. No changes in the AGE pathway in the kidney of type 1 and type 2 diabetic mouse models

(A) MG levels were determined using LC-MS/MS. **(B)** Glo1 gene expression, **(C, D)** protein level and **(E)** activity were measured using qPCR, WB analysis and a spetrophotometrical assay. For type 1 and type 2 diabetic study groups n = 6 or 5 (MG level), n = 8 or 4 (mRNA), n = 4 (protein), n = 5 or 4 (activity). Data is expressed as mean +/- SD. For statistical analysis two sided *t*-test was applied.

4.2.5   The polyol pathway was altered in a model-dependent manner: increase in type 1 and decrease in type 2 diabetes

Fructose, the endproduct of the polyol pathway, was increased in the BL6-STZ mice (1 +/- 0.27 vs 10.6 +/- 4.35 fold change, $p < 0.001$) but decreased in the db/db mice (1 +/- 0.27 vs 0.56 +/- 0.21 fold change, $p < 0.05$), (Figure 15).
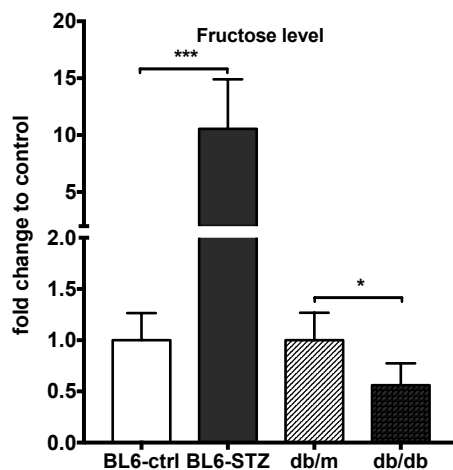
Figure 15. Model dependent alteration of the polyol pathway in the kidney of type 1 and type 2 diabetic mouse models

Intracellular fructose levels were quantified by liquid chromatography. For type 1 and type 2 diabetic study groups n = 6 or 4. Data is expressed as mean +/- SD. For statistical analysis two sided *t*-test was applied. * $p < 0.05$, *** $p < 0.001$ vs non-diabetic control.

4.2.6 The hexosamine pathway was altered in a model-dependent manner: increase in type 1 and decrease in type 2 diabetes

O-GlcNAc modifications were increased in the BL6-STZ mice (1 +/- 0.6 vs 3.5 +/- 1.0 fold change, $p < 0.01$) but decreased in the db/db mice (1 +/- 0.2 vs 0.4 +/- 0.1 fold change, $p < 0.01$), (Figure 16.A+B). This analysis showed a model-dependent change in the hexosamine pathway, which was independent of intracellular glucose and ROS-mediated inactivation of GAPDH.
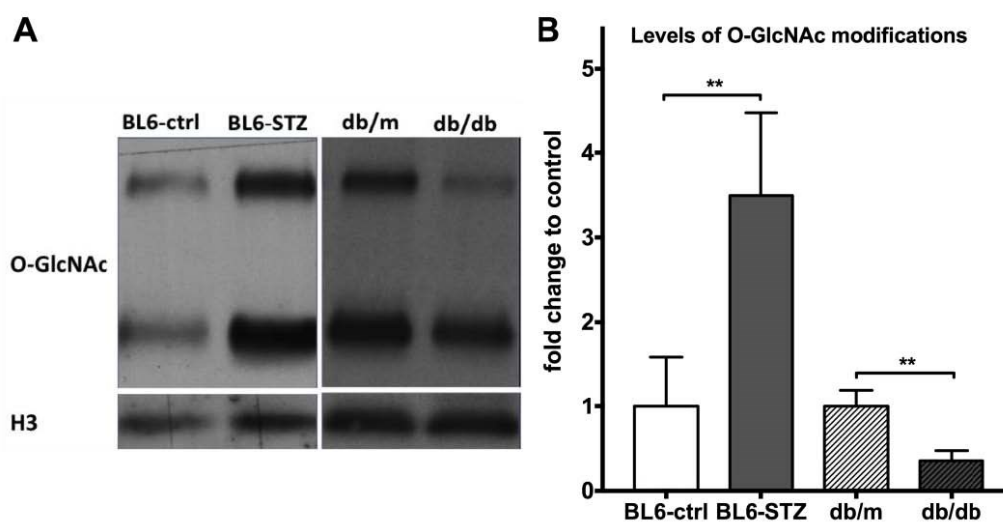
Figure 16. Altered O-linked β-*N*-acetylglucosamination in the kidney of type 1 diabetic and type 2 diabetic mouse models

(A) Levels of O-GlcNAc protein modifications were determined using WB. **(B)** Densitometry analysis of the two distinct bands showing O-GlcNAc modifications were performed and the fold change to the respective control was calculated. For type 1 and type 2 diabetic study groups n = 4. Data is expressed as mean +/- SD and two sided *t*-test was applied for statistical analysis ** $p < 0.01$ vs non-diabetic control.

4.3 Activation of NQO1 in the diabetic kidney

It was found that the mRNA levels of *Nrf2* were increased in the BL6-STZ mice (1 +/- 0.2 vs 1.6 +/- 0.4 fold change, p < 0.01), (Figure 17.A). As NRF2 activates the transcription of *Nqo1*, elevated mRNA levels of *Nrf2* resulted subsequently in an increased transcription of *Nqo1* in the BL6-STZ mice (1 +/- 0.3 vs 2.1 +/- 0.7 fold change, p < 0.01), (Figure 18.A). However, *Nrf2* and *Nqo1* mRNA levels remained unchanged in the kidney of the db/db mice (Figure 17.A). Next, it was analyzed whether the increase in mRNA level of *Nqo1* in the BL6-STZ mice was reflected in the protein level. NQO1 protein levels were increased in the BL6-STZ mice (1 +/- 0.2 vs 2.2 +/- 0.6 fold change, p < 0.05) but decreased in the db/db mice (1 +/- 0.3 vs 0.3 +/- 0.3 fold change, p < 0.01), (Figure 17.B+C). Finally, NQO1 activity was measured and was found to be elevated in both diabetic models (type 1: 1 +/- 0.1 vs 2.4 +/- 0.9 fold change, p < 0.001 and type 2: 1 +/- 0.1 vs 1.6 +/- 0.2 fold change, p < 0.05), (Figure 17.D). As the increase in NQO1 activity in the db/db mice was not reflected in the protein level, the NQO1 activity assay was performed including the specific inhibitor dicumarol to verify that only NQO1 activity was measured in the assay. Including the inhibitor, no NQO1 activity could be measured in any of the mouse models (data not shown).

The total NRF2/NQO1 pathway was only increased in the type 1 diabetic model, however, the activity of NQO1 was increased in both models. As such, the activity of NQO1 was the common alteration in the type 1 and type 2 diabetic mouse models, which were both affected by hyperglycemia and albuminuria.
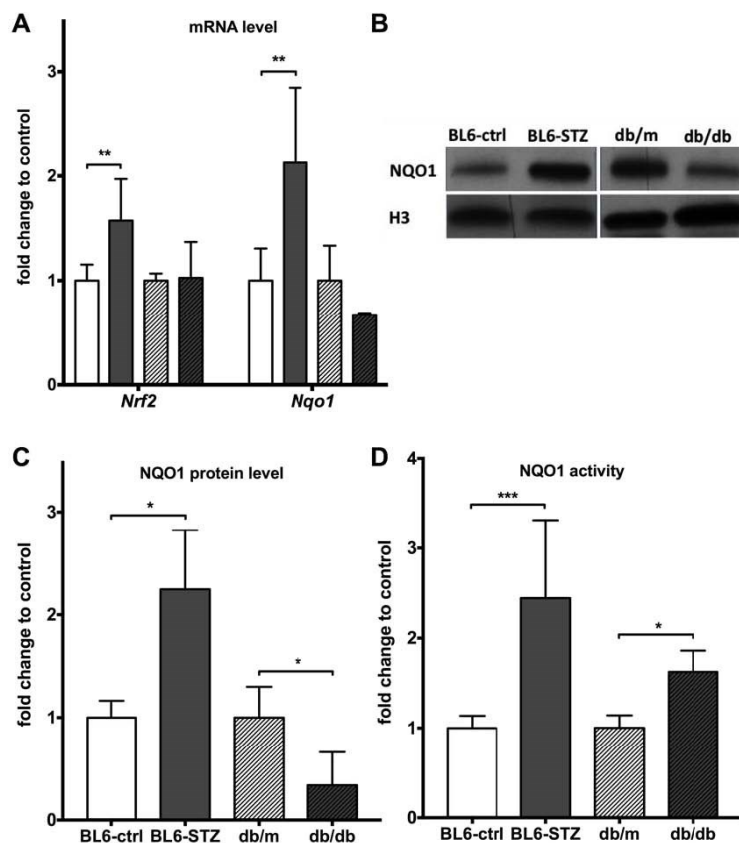
Figure 17. NQO1 levels and activity in the kidney of type 1 and type 2 diabetic mouse models

(A) *Nrf2* and *Nqo1* mRNA levels, **(B, C)** NQO1 protein level and **(D)** activity were measured using qPCR, WB and spetrophotometrical assays. For type 1 and type 2 diabetic study groups n = 8 and 4, respectively (mRNA), n = 4 (protein) and n = 5 and 4 respectively (activity). Data is expressed as mean +/- SD. For statistical analysis two sided *t*-test was applied * $p < 0.05$, ** $p < 0.01$ and *** $p < 0.001$ vs non-diabetic control.

5 Discussion

5.1 Diabetes-induced mitochondrial changes are tissue-specific

In this study, diabetes-induced mitochondrial changes were studied in 2 experimental murine models with 3 months of diabetes during which robust hyperglycemia was established. It was shown that changes to the mitochondria were tissue-, model- and substrate-specific and that the changes observed were in general not associated with each other. As such decreased O_2 consumption was not reflected in ATP production in the kidney of the db/db mice and increased O_2 consumption was not reflected in ATP and ROS production in the kidney of the STZ-treated mice. Moreover, there was no reflection of the intense increase in O_2 consumption in ATP production in the liver. This lack of association is in contradiction to the unifying theory, which describes a connection of elevated glucose levels to increased mitochondrial function. This subsequently leads to increased ROS levels, which cause cellular damage leading to the development of diabetic complications. However, the tissue specific and unassociated changes of the mitochondria, observed in this study, suggest that there is no unified response of the mitochondria to the diabetic condition.

Isolated mitochondria of the heart showed differences between the diabetic models with regard to ATP and O_2^- production. However, O_2 consumption was decreased in both models when succinate was used as a substrate for the ETC. Decreased O_2 consumption is consistent with previous studies in type 1 and type 2 diabetic models (Boudina et al., 2007; Bugger et al., 2008). During diabetes, it has been reported that the expression of the glucose transporter Glut4 was decreased in the heart resulting in increased fatty acid utilization (Wright et al., 2008). Fatty acids, however, are energetically detrimental as more O_2 is required for their oxidation, leading to increased myocardial O_2 consumption with reduced cardiac efficiency. This was shown in a diabetic rodent model as well as in insulin resistant and type 1 diabetic patients (How et al., 2006; Peterson, 2004; Peterson et al., 2008). Moreover, increased cardiac oxidation of fatty acids was associated with heart failure. A randomized clinical trial showed that partial inhibition of fatty acid oxidation

Discussion

improved ventricular function in patients with heart failure (Fragasso et al., 2006). Studies on O_2 consumption in saponin-permeabilized cardiac fibers of diabetic models showed that the mitochondria adapt to changes in substrate availability (Boudina et al., 2007; Bugger et al., 2008). Using glucose-derived substrates, O_2 consumption was reduced in Ins2$^{+/-}$ Akita mice after 10 weeks of diabetes. After longer duration of diabetes (24 weeks) this decrease was associated with decrease in ATP production. However, using fatty acids as substrates, neither O_2 consumption nor ATP production were changed (Bugger et al., 2008). O_2 consumption and ATP production were also decreased in saponin-permeabilized cardiac fibers of the db/db mice when glucose-derived substrates were used. The use of fatty acids, however, only decreased O_2 consumption and not ATP production in this model (Boudina et al., 2007). Both studies associated impaired oxidative phosphorylation with an increase in uncoupling proteins to adapt to the changes in substrate (Boudina et al., 2007; Bugger et al., 2008). These studies have shown, that the change of substrate availability from glucose to fatty acids led to a higher demand of O_2 and reduced cardiac efficiency. The mitochondria therefore adapted to this change with uncoupling as to have a better applicability for fatty acids. This would suggest that the decrease in O_2 consumption of the heart observed in the current study was associated with an adaption to fatty acids as substrates for oxidation. As such, the absence of glucose rather than its accumulation is involved in changes of the cardiac mitochondria leading to the development of cardiac complications in diabetes.

In the liver, despite increased plasma glucose, the glucose concentration was not increased in both diabetic models. However, O_2 consumption and O_2^- production increased in the isolated mitochondria when succinate was used as a substrate. Increased respiration in the liver is consistent with previous studies. In STZ-induced type 1 diabetic rats, elevated levels of complex I and II, but decreased levels of complex III and IV of the ETC were associated with increased O_2 consumption and ROS production of the mitochondria (Raza et al., 2011). O_2 consumption was increased in the mitochondria of wild type mice affected by high fat diet-induced T2D. Quantitative proteomic analysis showed that the functional changes were associated with elevated proteins of metabolic pathways such as the TCA cycle, fatty

Discussion

acid oxidation and oxidative phosphorylation (Guo et al., 2013). Increased expression of OXPHOS genes was also analyzed by microarray hybridization in the liver of insulin resistant mice. This increase was associated with elevated mitochondrial respiration (Buchner et al., 2011). Moreover, a clinical study showed increased transcription of OXPHOS genes in the liver of insulin-resistant patients (Misu et al., 2007). All of these studies associated altered insulin signaling with changes in the transcription of OXPHOS genes and subsequently increased mitochondrial respiration. This would suggest, that impaired insulin signaling rather than increased glucose levels can result in increased levels of OXPHOS proteins, which induce elevated mitochondrial O_2 consumption and O_2^- production, as observed in the current study.

The kidney of both diabetic models showed increased cellular glucose levels and increased albumin secretion. However, the changes in the mitochondria were model dependent. ATP production and O_2 consumption were increased in the type 1 diabetic model, whereas O_2 consumption decreased in the type 2 diabetic model. Increased glucose levels, therefore, cannot be responsible for the model-dependent differences observed. Moreover, increased glucose cannot be considered to cause mitochondrial ROS production as despite increased glucose, both models, showed no increase in mitochondrial O_2^- and H_2O_2 production. Unchanged mitochondrial ROS production, however, is contradictory to the majority of studies, which have reported an increase in renal ROS production *ex vivo* (Abdo et al., 2014; de Cavanagh et al., 2008; Coughlan et al., 2016; Fujita et al., 2012; Palsamy and Subramanian, 2011), (Appendix, Table 8). These studies associate elevated ROS levels with the development of cellular damage. However, Dugan et al. showed, that ROS production decreased *in vivo* and in isolated mitochondria of STZ-induced diabetic mice. Moreover, decrease in a ROS detoxification enzyme in diabetic *Sod2*$^{+/-}$ mice did not worsen albumin secretion. In this model, increase in O_2^- were even associated with reduction of albumin secretion (Dugan et al., 2013). These studies suggest that the cellular response to ROS exposure is not linear but dose-dependent with low doses of ROS being beneficial but higher doses being harmful (Ristow and Schmeisser, 2014). In the current study, changes in mitochondrial function were analyzed after 3 months of diabetes. At this time point mitochondrial ROS

production was not increased. However, it cannot be ruled out that ROS levels increase after longer duration of diabetes and contribute to the pathogenesis of diabetic complications. Therefore, ROS production should be analyzed after a longer duration of diabetes to determine whether increased oxidative stress is involved in later stages of nephropathy.

The current study analyzed functional changes in isolated mitochondria using previously described protocols (Will et al., 2007). However, it needs to be considered that potential diabetes-induced changes of cofactors like the NAD^+/NADH ratio, which can exist *in vivo*, are not represented in the isolated system. As such, it cannot be excluded that the experimental set up did not reflect the exact conditions found *in vivo*. As such, improper buffer composition could explain, why most changes in mitochondrial function were only detectable when succinate was used as a substrate for the ETC. The results obtained in the current study should, therefore, be verified in a now available transgenic mouse expressing a redox-sensitive H_2O_2 biosensor, which is targeted to the mitochondria (Fujikawa et al., 2016).

5.2 The unifying theory is not applicable to the early stages of nephropathy

The kidneys of both diabetic models were affected by albuminuria and by increased levels of intracellular glucose. Despite the changes in mitochondrial function, ROS production was not increased in the mitochondria. Oxidative stress was also analyzed in renal tissue. As ROS have a short half-life, they are precarious to measure in whole tissue. Previous studies have shown that increased ROS levels correlate negatively with the activity of the antioxidant defense mechanism (Furukawa et al., 2004; Sam et al., 2005). Therefore, changes in the antioxidant defense system were measured in this study to assess the oxidative stress level in renal cell lysate. SOD activity remained unchanged in both models whereas CAT activity decreased in the db/db model suggesting that there is no oxidative stress in the STZ-model and mild oxidative stress in the db/db model. However, the potentially increased H_2O_2 levels in the db/db mice did not result in ROS-induced inactivation of GAPDH activity. If the unifying theory were correct the pathways of

hyperglycemic damage could not become activated without ROS-mediated inactivation of GAPDH activity. As both diabetic models were affected by early stages of nephropathy, it was therefore analyzed, whether there is a GAPDH independent activation of the major pathways described for cellular damage induced by hyperglycemia. Regarding the triosephosphate-depending pathways, total PKC activity was unchanged. Moreover, MG was not significantly increased and the activity of its detoxifying enzyme remained unchanged, suggesting that the AGE pathway remained inactivated as well. As such the triosephosphate-depending pathways of the unifying theory (PKC and AGE) remained inactivated without ROS-mediated decrease in GAPDH activity. This is in agreement with the unifying theory, suggesting that indeed ROS is required for the inactivation of GAPDH and subsequent activation of the PKC and the AGE pathway. The development of nephropathy without activation of the pathways of hyperglycemic damage, however, is inconsistent with this theory (Brownlee, 2001). The inconsistency with the unifying theory would explain, why most clinical trials using antioxidants or inhibitors of the pathways showed no benefit with regard to the pathogenesis of nephropathy. The urinary albumin secretion rate was decreased in a small trial treating T2D patients with a combination of the antioxidants vitamin C and vitamin E for 4 weeks (Gaede et al., 2001). However, a larger cohort, involving more than 3000 diabetic patients, showed no benefit on nephropathy or cardiovascular outcome after more than 4 years of treatment with vitamin E (Lonn et al., 2002). Treatment with the synthetic vitamin B_1 benfotiamine, an AGE lowering drug, (900 mg/day) for 3 months showed no benefit of nephropathy symptoms in T2D (Alkhalaf et al., 2010). Moreover, the PKC inhibitor ruboxistaurin, did not improve symptoms of nephropathy in a large diabetic study cohort after 3 years of treatment (Tuttle et al., 2007, 2015). Unlike in the kidney, however, studies have shown the activation of pathways of hyperglycemic damage in other organs such as retina and neurons (Hammes et al., 2003; Madsen-Bouterse et al., 2010; Nakamura et al., 1999; Obrosova et al., 2004). In these tissues therapies inhibiting the activation of the pathways of hyperglycemic damage were beneficial. The PKC inhibitor ruboxistaurin has been shown to have a beneficial effect on vision loss in the context of retinopathy (Aiello et al., 2011). Regarding neuropathy, Casellini et al. reported

Discussion

improved symptoms of peripheral neuropathy after 6 months of treatment with ruboxistaurin (Casellini et al., 2007). These studies provide further support that diabetes induces organ-specific changes, which lead to the activation of pathways described for hyperglycemia-induced cellular damage in tissues including neurons and retina. In early stages of nephropathy, however, ROS-induced activation of the pathways was not detected in total kidney lysate. The kidney is composed of different cell types and in this work a mixture of all renal cells was analyzed. As such, the proximal tubule epithelial cells, which are the most abundant cell type in the kidney, represent the majority of cells analyzed in total kidney lysates (Nakhoul and Batuman, 2011). Further studies are therefore required to determine whether ROS-mediated activation of the pathways of cellular damage is present in a small subset of distinct cell types in the diabetic kidney.

The pathways upstream of triosephosphates were activated in a model-dependent manner. Despite the symptoms of nephropathy in both models, the levels of fructose, the endproduct of the polyol pathway, were increased in the STZ-model and decreased in the db/db model. According to the unifying theory, glucose is directly utilized in the polyol pathway. Despite increased renal glucose levels in both models, however, only the type 1 diabetic model showed ROS-independent activation of the polyol pathway. As such the activation of the polyol pathway cannot be glucose dependent, which is consistent with the previously reported high K_m value of aldose reductase, the first enzyme of the polyol pathway, for glucose ($K_m = 100$ mM) (Bohren et al., 1992). This suggests, that another substrate has been used by aldose reductase to increase the levels of fructose in the type 1 diabetic model. Further studies are, therefore, required to determine the substrate for the activation of the polyol pathway in T1D.

The activation of the hexosamine pathway was also model-dependent. The endproduct of this pathway is uridine diphosphate N-actelyglucosamine, which can modify proteins resulting in O-linked β-*N*-acetylglucosamination (O-GlcNAc). The O-GlcNAc levels were increased in the type 1 diabetic but decreased in the type 2 diabetic model. Despite elevated renal glucose levels in both models, the changes of the hexosamine pathway were model-dependent and can, therefore, not be

associated with intracellular glucose concentrations or ROS- mediated inactivation of GAPDH.

The model-dependent changes in the polyol and hexosamine pathway, which were first reported in this study, are inconsistent with the unifying theory. As both models are affected by increased renal glucose concentrations, the differences in the activation of the pathways cannot be explained by hyperglycemia. Moreover, the polyol and the AGE pathway cannot be considered to be involved in the pathogenesis of diabetic kidney disease as these pathways were only activated in the type 1 diabetic model, whereas both models were affected by symptoms of early nephropathy. As such the mechanisms involved in the development of diabetes-associated kidney disease are still not fully understood.

5.3   Increased NQO1 activity in the early stages of nephropathy

The unifying theory cannot be applied to the development of the symptoms of early nephropathy, as oxidative stress is not increased in the diabetic kidney. As such other mechanisms must be involved in the pathogenesis of diabetic kidney disease. Recently, it has been published, that NQO1 activity attenuates kidney injury (Oh et al., 2014). NQO1 is a classical reporter gene for the activity of NRF2, a transcription factor which is induced by cellular stress. However, the type of cellular stress, which activates NRF2, is under debate. Studies have reported that NRF2 is activated by oxidative stress but also by ROS-independent pathways such as during the inflammatory response (Nguyen et al., 2009; Rushworth et al., 2008). As diabetes is associated with chronic inflammation, the activation of the NRF2/NQO1 pathway was analyzed as a possible oxidative stress-independent mechanism activated in nephropathy. The mRNA levels of NRF2 and NQO1 were increased in the kidney of the type 1 but not of the type 2 diabetic model. Increased levels of NRF2 and NQO1 in T1D are consistent with previous studies, which reported elevated NRF2 and NQO1 levels in kidneys of diabetic patients with proteinuria and type 1 diabetic wild type mice (Jiang et al., 2010). In the current study, however, mRNA and protein levels of NRF2 and NQO1 were not increased in T2D. Nevertheless, the activity of NQO1 was increased in both diabetic models. Increased NQO1 activity suggests that there is an oxidative stress independent cellular stressor in diabetes, which is not

Discussion

activating the pathways of the unifying theory but is leading to the activation of NRF2 and NQO1. NQO1 utilizes NAD(P)H and catalyzes the two electron reduction of quinones to quinols whereby the cellular $NAD(P)^+/NAD(P)H$ ratio is increased (Ross and Siegel, 2004). Ubiquinone levels have been reported to be increased in the plasma of patients with T2D (Ates et al., 2013). Moreover, treatment of $Ins2^{+/-}$ Akita mice with the mitochondria-targeted ubiquinone MitoQ, a substrate of NQO1, improved glomerular function and albumin secretion (Chacko et al., 2010). Increased activity of NQO1 and increased $NAD(P)^+/NAD(P)H$ ratio were also associated with improved serum creatinine levels and decreased kidney injury (Oh et al., 2014). These studies suggest, that increased levels of ubiquinone result in increased activity of NQO1 and increased $NAD(P)^+/NAD(P)H$ ratio causing beneficial effects to prevent the development of diabetic complications. Despite increased activity of NQO1, however, the diabetic mice, assessed in this study, developed albuminuria. As such, a NQO1 knockout model needs to be assessed in the context of diabetes to determine whether increased activity of NQO1 has a beneficial effect in the development of nephropathy and whether NQO1 could be a promising target in the development of an anti-diabetic drug.

6 Summary

The development of diabetic complications has been associated with glucose-induced increased mitochondrial ROS production and subsequently activation of four major pathways described in the unifying theory such as the polyol, the hexosamine, the protein kinase C (PKC) and the advanced glycation endproduct (AGE) pathway. However, intensive glucose therapy was only beneficial for a small subset of patients. Moreover, experimental studies have not been able to clarify whether the function of the mitochondria was changed in diabetes resulting in increased ROS production. The results depended on the tissue assessed and methods used. This study therefore, used the same methods to analyze mitochondrial changes in different tissues of 3 months diabetic streptozotocin (STZ)-induced C57BL/6 and db/db mice, along with the respective age-matched controls. Diabetes-induced changes of isolated mitochondria were model, tissue and substrate specific. However, some changes were found to be independent of the diabetes type. These changes included decreased O_2 consumption in the diabetic heart as well as increased O_2 consumption and O_2^- production in the diabetic liver. Regarding the kidney of both models, ROS production remained unchanged, despite elevated renal glucose levels and increased albumin secretion in the urine. As a consequence of the absence of oxidative stress, GAPDH was not inactivated. Moreover, the PKC and the AGE pathway were not altered in the diabetic kidneys. Absence of activation of these two pathways without increase in ROS production was consistent with the unifying theory, however, ROS-independent development of albuminuria was not consistent with this theory. Moreover, it was inconsistent with the unifying theory that the hexosamine and the polyol pathway were ROS-independently activated in the STZ-model. Both pathways were not activated in the db/db model and their activation can therefore not be involved in the development of albuminuria. As such, the unifying theory cannot explain the situation in the early phase of nephropathy. With regard to the activation of potential protective mechanism against the development of diabetic complications this study could show increased activation of NAD(P)H quinone reductase (NQO1) in the kidney of both diabetic models. Increased activity of NQO1 has previously been shown to mitigate kidney damage. However, the exact

Summary

mechanisms for this activation need to be further analyzed to determine whether NQO1 mitigates diabetic kidney disease and whether it is a potential target for an anti-diabetic therapy.

NQO1 mitigates diabetic kidney disease and whether it is a potential target for an anti-diabetic therapy.

References

7 References

Abdo, S., Shi, Y., Otoukesh, A., Ghosh, A., Lo, C.-S., Chenier, I., Filep, J.G., Ingelfinger, J.R., Zhang, S.L., and Chan, J.S.D. (2014). Catalase Overexpression Prevents Nuclear Factor Erythroid 2-Related Factor 2 Stimulation of Renal Angiotensinogen Gene Expression, Hypertension, and Kidney Injury in Diabetic Mice. Diabetes *63*, 3483–3496.

Aiello, L.P., Vignati, L., Sheetz, M.J., Zhi, X., Girach, A., Davis, M.D., Wolka, A.M., Shahri, N., and Milton, R.C. (2011). ORAL PROTEIN KINASE C β INHIBITION USING RUBOXISTAURIN: Efficacy, Safety, and Causes of Vision Loss Among 813 Patients (1,392 Eyes) with Diabetic Retinopathy in the Protein Kinase C β Inhibitor-Diabetic Retinopathy Study and the Protein kinase C β Inhibitor-Diabetic Retinopathy Study 2. Retina *31*, 2084–2094.

Alberti, K.G., and Zimmet, P.Z. (1998). Definition, diagnosis and classification of diabetes mellitus and its complications. Part 1: diagnosis and classification of diabetes mellitus provisional report of a WHO consultation. Diabet. Med. J. Br. Diabet. Assoc. *15*, 539–553.

Aliciguzel, Y., Ozen, I., Aslan, M., and Karayalcin, U. (2003). Activities of xanthine oxidoreductase and antioxidant enzymes in different tissues of diabetic rats. J. Lab. Clin. Med. *142*, 172–177.

Alkhalaf, A., Klooster, A., van Oeveren, W., Achenbach, U., Kleefstra, N., Slingerland, R.J., Mijnhout, G.S., Bilo, H.J.G., Gans, R.O.B., Navis, G.J., et al. (2010). A Double-Blind, Randomized, Placebo-Controlled Clinical Trial on Benfotiamine Treatment in Patients With Diabetic Nephropathy. Diabetes Care *33*, 1598–1601.

Ates, O., Bilen, H., Keles, S., Alp, H.H., Keleş, M.S., Yıldırım, K., Öndaş, O., Pınar, L.C., Civelekler, M., and Baykal, O. (2013). Plasma coenzyme Q10 levels in type 2 diabetic patients with retinopathy. Int. J. Ophthalmol. *6*, 675–679.

Atorino, L., Di Meglio, S., Farina, B., Jones, R., and Quesada, P. (2001). Rat germinal cells require PARP for repair of DNA damage induced by gamma-irradiation and H2O2 treatment. Eur. J. Cell Biol. *80*, 222–229.

Barati, M.T., Merchant, M.L., Kain, A.B., Jevans, A.W., McLeish, K.R., and Klein, J.B. (2007). Proteomic analysis defines altered cellular redox pathways and advanced glycation end-product metabolism in glomeruli of db/db diabetic mice. Am. J. Physiol. Renal Physiol. *293*, F1157–F1165.

Beers, R.F., and Sizer, I.W. (1952). A spectrophotometric method for measuring the breakdown of hydrogen peroxide by catalase. J. Biol. Chem. *195*, 133–140.

References

Beisswenger, P.J., Drummond, K.S., Nelson, R.G., Howell, S.K., Szwergold, B.S., and Mauer, M. (2005). Susceptibility to Diabetic Nephropathy Is Related to Dicarbonyl and Oxidative Stress. Diabetes *54*, 3274–3281.

Bergmeyer, H.U., Gawehn, K., and Grassl, M. (1974). In Methods of Enzymatic Analysis, H.U. Bergmeyer, ed. (New York, NY: Academic Press, Inc.), pp. 466–467.

Bierhaus, A., Humpert, P.M., Morcos, M., Wendt, T., Chavakis, T., Arnold, B., Stern, D.M., and Nawroth, P.P. (2005). Understanding RAGE, the receptor for advanced glycation end products. J. Mol. Med. Berl. Ger. *83*, 876–886.

Bierhaus, A., Fleming, T., Stoyanov, S., Leffler, A., Babes, A., Neacsu, C., Sauer, S.K., Eberhardt, M., Schnölzer, M., Lasitschka, F., et al. (2012). Methylglyoxal modification of Nav1.8 facilitates nociceptive neuron firing and causes hyperalgesia in diabetic neuropathy. Nat. Med. *18*, 926–933.

Birben, E., Sahiner, U.M., Sackesen, C., Erzurum, S., and Kalayci, O. (2012). Oxidative Stress and Antioxidant Defense: World Allergy Organ. J. *5*, 9–19.

Bohren, K.M., Grimshaw, C.E., and Gabbay, K.H. (1992). Catalytic effectiveness of human aldose reductase. Critical role of C-terminal domain. J. Biol. Chem. *267*, 20965–20970.

Boudina, S., Sena, S., Theobald, H., Sheng, X., Wright, J.J., Hu, X.X., Aziz, S., Johnson, J.I., Bugger, H., Zaha, V.G., et al. (2007). Mitochondrial Energetics in the Heart in Obesity-Related Diabetes Direct Evidence for Increased Uncoupled Respiration and Activation of Uncoupling Proteins. Diabetes *56*, 2457–2466.

Bradford, M.M. (1976). A rapid and sensitive method for the quantitation of microgram quantities of protein utilizing the principle of protein-dye binding. Anal. Biochem. *72*, 248–254.

Brand, M.D., Affourtit, C., Esteves, T.C., Green, K., Lambert, A.J., Miwa, S., Pakay, J.L., and Parker, N. (2004). Mitochondrial superoxide: production, biological effects, and activation of uncoupling proteins. Free Radic. Biol. Med. *37*, 755–767.

Brownlee, M. (2001). Biochemistry and molecular cell biology of diabetic complications. Nature *414*, 813–820.

Brownlee, M. (2005). The pathobiology of diabetic complications: a unifying mechanism. Diabetes *54*, 1615–1625.

References

Buchner, D.A., Yazbek, S.N., Solinas, P., Burrage, L.C., Morgan, M.G., Hoppel, C.L., and Nadeau, J.H. (2011). Increased Mitochondrial Oxidative Phosphorylation in the Liver Is Associated With Obesity and Insulin Resistance. Obesity *19*, 917–924.

Bugger, H., Boudina, S., Hu, X.X., Tuinei, J., Zaha, V.G., Theobald, H.A., Yun, U.J., McQueen, A.P., Wayment, B., Litwin, S.E., et al. (2008). Type 1 diabetic akita mouse hearts are insulin sensitive but manifest structurally abnormal mitochondria that remain coupled despite increased uncoupling protein 3. Diabetes *57*, 2924–2932.

Bugger, H., Chen, D., Riehle, C., Soto, J., Theobald, H.A., Hu, X.X., Ganesan, B., Weimer, B.C., and Abel, E.D. (2009). Tissue-specific remodeling of mitochondrial proteome in type 1 diabetic akita mice. Diabetes *58*, 1986–1997.

Bugger, H., Riehle, C., Jaishy, B., Wende, A.R., Tuinei, J., Chen, D., Soto, J., Pires, K.M., Boudina, S., Theobald, H.A., et al. (2012). Genetic loss of insulin receptors worsens cardiac efficiency in diabetes. J. Mol. Cell. Cardiol. *52*, 1019–1026.

Bürstenbinder, K., Rzewuski, G., Wirtz, M., Hell, R., and Sauter, M. (2007). The role of methionine recycling for ethylene synthesis in Arabidopsis: Ethylene synthesis and methionine recycling. Plant J. *49*, 238–249.

Cai, D., Yuan, M., Frantz, D.F., Melendez, P.A., Hansen, L., Lee, J., and Shoelson, S.E. (2005). Local and systemic insulin resistance resulting from hepatic activation of IKK-β and NF-κB. Nat. Med. *11*, 183–190.

Casellini, C.M., Barlow, P.M., Rice, A.L., Casey, M., Simmons, K., Pittenger, G., Bastyr, E.J., Wolka, A.M., and Vinik, A.I. (2007). A 6-Month, Randomized, Double-Masked, Placebo-Controlled Study Evaluating the Effects of the Protein Kinase C- Inhibitor Ruboxistaurin on Skin Microvascular Blood Flow and Other Measures of Diabetic Peripheral Neuropathy. Diabetes Care *30*, 896–902.

de Cavanagh, E.M.V., Ferder, L., Toblli, J.E., Piotrkowski, B., Stella, I., Fraga, C.G., and Inserra, F. (2008). Renal mitochondrial impairment is attenuated by AT1 blockade in experimental Type I diabetes. Am. J. Physiol. Heart Circ. Physiol. *294*, H456–H465.

Chacko, B.K., Reily, C., Srivastava, A., Johnson, M.S., Ye, Y., Ulasova, E., Agarwal, A., Zinn, K.R., Murphy, M.P., Kalyanaraman, B., et al. (2010). Prevention of diabetic nephropathy in Ins2+/−AkitaJ mice by the mitochondria-targeted therapy MitoQ. Biochem. J. *432*, 9–19.

Chelikani, P., Fita, I., and Loewen, P.C. (2004). Diversity of structures and properties among catalases. Cell. Mol. Life Sci. CMLS *61*, 192–208.

References

Chung, S.S.M., Ho, E.C.M., Lam, K.S.L., and Chung, S.K. (2003). Contribution of polyol pathway to diabetes-induced oxidative stress. J. Am. Soc. Nephrol. JASN *14*, S233–S236.

Coughlan, M.T., Cooper, M.E., and Forbes, J.M. (2007). Renal Microvascular Injury in Diabetes: RAGE and Redox Signaling. Antioxid. Redox Signal. *9*, 331–342.

Coughlan, M.T., Nguyen, T.-V., Penfold, S.A., Higgins, G.C., Thallas-Bonke, V., Tan, S.M., Van Bergen, N.J., Sourris, K.C., Harcourt, B.E., Thorburn, D.R., et al. (2016). Mapping time-course mitochondrial adaptations in the kidney in experimental diabetes. Clin. Sci. *130*, 711–720.

Cox, B., and Emili, A. (2006). Tissue subcellular fractionation and protein extraction for use in mass-spectrometry-based proteomics. Nat. Protoc. *1*, 1872–1878.

Dagher, Z., Park, Y.S., Asnaghi, V., Hoehn, T., Gerhardinger, C., and Lorenzi, M. (2004). Studies of rat and human retinas predict a role for the polyol pathway in human diabetic retinopathy. Diabetes *53*, 2404–2411.

Daneman, D. (2006). Type 1 diabetes. Lancet Lond. Engl. *367*, 847–858.

Davies, J.L., Kawaguchi, Y., Bennett, S.T., Copeman, J.B., Cordell, H.J., Pritchard, L.E., Reed, P.W., Gough, S.C.L., Jenkins, S.C., Palmer, S.M., et al. (1994). A genome-wide search for human type 1 diabetes susceptibility genes. Nature *371*, 130–136.

DCCT/EDIC Research Group (2011). Intensive Diabetes Therapy and Glomerular Filtration Rate in Type 1 Diabetes. N. Engl. J. Med. *365*, 2366–2376.

DCCT Research Group (1995). Effect of intensive therapy on the development and progression of diabetic nephropathy in the Diabetes Control and Complications Trial. The Diabetes Control and Complications (DCCT) Research Group. Kidney Int. *47*, 1703–1720.

DeRubertis, F.R., Craven, P.A., Melhem, M.F., and Salah, E.M. (2004). Attenuation of renal injury in db/db mice overexpressing superoxide dismutase: evidence for reduced superoxide-nitric oxide interaction. Diabetes *53*, 762–768.

Dobler, D., Ahmed, N., Song, L., Eboigbodin, K.E., and Thornalley, P.J. (2006). Increased Dicarbonyl Metabolism in Endothelial Cells in Hyperglycemia Induces Anoikis and Impairs Angiogenesis by RGD and GFOGER Motif Modification. Diabetes *55*, 1961–1969.

Drose, S., and Brandt, U. (2008). The Mechanism of Mitochondrial Superoxide Production by the Cytochrome bc1 Complex. J. Biol. Chem. *283*, 21649–21654.

References

Du, X., Matsumura, T., Edelstein, D., Rossetti, L., Zsengellér, Z., Szabó, C., and Brownlee, M. (2003). Inhibition of GAPDH activity by poly(ADP-ribose) polymerase activates three major pathways of hyperglycemic damage in endothelial cells. J. Clin. Invest. *112*, 1049–1057.

Du, X.-L., Edelstein, D., Rossetti, L., Fantus, I.G., Goldberg, H., Ziyadeh, F., Wu, J., and Brownlee, M. (2000). Hyperglycemia-induced mitochondrial superoxide overproduction activates the hexosamine pathway and induces plasminogen activator inhibitor-1 expression by increasing Sp1 glycosylation. Proc. Natl. Acad. Sci. *97*, 12222–12226.

Dugan, L.L., You, Y.-H., Ali, S.S., Diamond-Stanic, M., Miyamoto, S., DeCleves, A.-E., Andreyev, A., Quach, T., Ly, S., Shekhtman, G., et al. (2013). AMPK dysregulation promotes diabetes-related reduction of superoxide and mitochondrial function. J. Clin. Invest. *123*, 4888–4899.

Eberhardt, M.J., Filipovic, M.R., Leffler, A., de la Roche, J., Kistner, K., Fischer, M.J., Fleming, T., Zimmermann, K., Ivanovic-Burmazovic, I., Nawroth, P.P., et al. (2012). Methylglyoxal activates nociceptors through transient receptor potential channel A1 (TRPA1): a possible mechanism of metabolic neuropathies. J. Biol. Chem. *287*, 28291–28306.

Fragasso, G., Palloshi, A., Puccetti, P., Silipigni, C., Rossodivita, A., Pala, M., Calori, G., Alfieri, O., and Margonato, A. (2006). A Randomized Clinical Trial of Trimetazidine, a Partial Free Fatty Acid Oxidation Inhibitor, in Patients With Heart Failure. J. Am. Coll. Cardiol. *48*, 992–998.

Francescato, M.P., Stel, G., Geat, M., and Cauci, S. (2014). Oxidative Stress in Patients with Type 1 Diabetes Mellitus: Is It Affected by a Single Bout of Prolonged Exercise? PLOS ONE *9*, e99062.

Franko, A., von Kleist-Retzow, J.-C., Neschen, S., Wu, M., Schommers, P., Böse, M., Kunze, A., Hartmann, U., Sanchez-Lasheras, C., Stoehr, O., et al. (2014). Liver adapts mitochondrial function to insulin resistant and diabetic states in mice. J. Hepatol. *60*, 816–823.

Fujikawa, Y., Roma, L.P., Sobotta, M.C., Rose, A.J., Diaz, M.B., Locatelli, G., Breckwoldt, M.O., Misgeld, T., Kerschensteiner, M., Herzig, S., et al. (2016). Mouse redox histology using genetically encoded probes. Sci. Signal. *9*, rs1–rs1.

Fujita, H., Fujishima, H., Morii, T., Sakamoto, T., Komatsu, K., Hosoba, M., Narita, T., Takahashi, K., Takahashi, T., and Yamada, Y. (2012). Modulation of renal superoxide dismutase by telmisartan therapy in C57BL/6-Ins2(Akita) diabetic mice. Hypertens. Res. Off. J. Jpn. Soc. Hypertens. *35*, 213–220.

References

Furukawa, S., Fujita, T., Shimabukuro, M., Iwaki, M., Yamada, Y., Nakajima, Y., Nakayama, O., Makishima, M., Matsuda, M., and Shimomura, I. (2004). Increased oxidative stress in obesity and its impact on metabolic syndrome. J. Clin. Invest. *114*, 1752–1761.

Gaede, P., Poulsen, H.E., Parving, H.-H., and Pedersen, O. (2001). Double-blind, randomised study of the effect of combined treatment with vitamin C and E on albuminuria in Type 2 diabetic patients. Diabet. Med. *18*, 756–760.

Geraldes, P., and King, G.L. (2010). Activation of Protein Kinase C Isoforms and Its Impact on Diabetic Complications. Circ. Res. *106*, 1319–1331.

Giacco, F., and Brownlee, M. (2010). Oxidative Stress and Diabetic Complications. Circ. Res. *107*, 1058–1070.

Gille, L., and Nohl, H. (2001). The ubiquinol/bc1 redox couple regulates mitochondrial oxygen radical formation. Arch. Biochem. Biophys. *388*, 34–38.

Godin, D.V., Wohaieb, S.A., Garnett, M.E., and Goumeniouk, A.D. (1988). Antioxidant enzyme alterations in experimental and clinical diabetes. Mol. Cell. Biochem. *84*, 223–231.

Guo, Y., Darshi, M., Ma, Y., Perkins, G.A., Shen, Z., Haushalter, K.J., Saito, R., Chen, A., Lee, Y.S., Patel, H.H., et al. (2013). Quantitative Proteomic and Functional Analysis of Liver Mitochondria from High Fat Diet (HFD) Diabetic Mice. Mol. Cell. Proteomics *12*, 3744–3758.

Guzik, T.J., Mussa, S., Gastaldi, D., Sadowski, J., Ratnatunga, C., Pillai, R., and Channon, K.M. (2002). Mechanisms of increased vascular superoxide production in human diabetes mellitus: role of NAD(P)H oxidase and endothelial nitric oxide synthase. Circulation *105*, 1656–1662.

Halliwell, B. (2006). Reactive Species and Antioxidants. Redox Biology Is a Fundamental Theme of Aerobic Life. PLANT Physiol. *141*, 312–322.

Hammes, H.-P., Du, X., Edelstein, D., Taguchi, T., Matsumura, T., Ju, Q., Lin, J., Bierhaus, A., Nawroth, P., Hannak, D., et al. (2003). Benfotiamine blocks three major pathways of hyperglycemic damage and prevents experimental diabetic retinopathy. Nat. Med. *9*, 294–299.

Hara, M.R., Agrawal, N., Kim, S.F., Cascio, M.B., Fujimuro, M., Ozeki, Y., Takahashi, M., Cheah, J.H., Tankou, S.K., Hester, L.D., et al. (2005). S-nitrosylated GAPDH initiates apoptotic cell death by nuclear translocation following Siah1 binding. Nat. Cell Biol. *7*, 665–674.

References

Harris, M.I., Klein, R., Welborn, T.A., and Knuiman, M.W. (1992). Onset of NIDDM occurs at least 4-7 yr before clinical diagnosis. Diabetes Care *15*, 815–819.

He, X., Chen, M.G., Lin, G.X., and Ma, Q. (2006). Arsenic Induces NAD(P)H-quinone Oxidoreductase I by Disrupting the Nrf2{middle dot}Keap1{middle dot}Cul3 Complex and Recruiting Nrf2{middle dot}Maf to the Antioxidant Response Element Enhancer. J. Biol. Chem. *281*, 23620–23631.

Holmström, K.M., and Finkel, T. (2014). Cellular mechanisms and physiological consequences of redox-dependent signalling. Nat. Rev. Mol. Cell Biol. *15*, 411–421.

How, O.-J., Aasum, E., Severson, D.L., Chan, W.Y.A., Essop, M.F., and Larsen, T.S. (2006). Increased myocardial oxygen consumption reduces cardiac efficiency in diabetic mice. Diabetes *55*, 466–473.

Hruz, T., Wyss, M., Docquier, M., Pfaffl, M.W., Masanetz, S., Borghi, L., Verbrugghe, P., Kalaydjieva, L., Bleuler, S., Laule, O., et al. (2011). RefGenes: identification of reliable and condition specific reference genes for RT-qPCR data normalization. BMC Genomics *12*, 156.

Hummel, K.P., Dickie, M.M., and Coleman, D.L. (1966). Diabetes, a new mutation in the mouse. Science *153*, 1127–1128.

Ismail-Beigi, F., Craven, T., Banerji, M.A., Basile, J., Calles, J., Cohen, R.M., Cuddihy, R., Cushman, W.C., Genuth, S., Grimm, R.H., et al. (2010). Effect of intensive treatment of hyperglycaemia on microvascular outcomes in type 2 diabetes: an analysis of the ACCORD randomised trial. Lancet Lond. Engl. *376*, 419–430.

Jena, N.R. (2012). DNA damage by reactive species: Mechanisms, mutation and repair. J. Biosci. *37*, 503–517.

Jiang, T., Huang, Z., Lin, Y., Zhang, Z., Fang, D., and Zhang, D.D. (2010). The protective role of Nrf2 in streptozotocin-induced diabetic nephropathy. Diabetes *59*, 850–860.

Kahn, S.E., Cooper, M.E., and Prato, S.D. (2014). Pathophysiology and treatment of type 2 diabetes: perspectives on the past, present, and future. The Lancet *383*, 1068–1083.

Kakkar, R., Mantha, S.V., Radhi, J., Prasad, K., and Kalra, J. (1998). Increased oxidative stress in rat liver and pancreas during progression of streptozotocin-induced diabetes. Clin. Sci. Lond. Engl. 1979 *94*, 623–632.

Kanwar, M., and Kowluru, R.A. (2009). Role of Glyceraldehyde 3-Phosphate Dehydrogenase in the Development and Progression of Diabetic Retinopathy. Diabetes *58*, 227–234.

References

Keaney, J.F. (2003). Obesity and Systemic Oxidative Stress: Clinical Correlates of Oxidative Stress in The Framingham Study. Arterioscler. Thromb. Vasc. Biol. *23*, 434–439.

Kotlyar, A.B., Sled, V.D., Burbaev, D.S., Moroz, I.A., and Vinogradov, A.D. (1990). Coupling site I and the rotenone-sensitive ubisemiquinone in tightly coupled submitochondrial particles. FEBS Lett. *264*, 17–20.

Krishnamoorthy, G., and Hinkle, P.C. (1988). Studies on the electron transfer pathway, topography of iron-sulfur centers, and site of coupling in NADH-Q oxidoreductase. J. Biol. Chem. *263*, 17566–17575.

Kudin, A.P. (2003). Characterization of Superoxide-producing Sites in Isolated Brain Mitochondria. J. Biol. Chem. *279*, 4127–4135.

Kushnareva, Y., Murphy, A.N., and Andreyev, A. (2002). Complex I-mediated reactive oxygen species generation: modulation by cytochrome c and NAD(P)+ oxidation–reduction state. Biochem. J. *368*, 545–553.

Kussmaul, L., and Hirst, J. (2006). The mechanism of superoxide production by NADH:ubiquinone oxidoreductase (complex I) from bovine heart mitochondria. Proc. Natl. Acad. Sci. *103*, 7607–7612.

Laemmli, U.K. (1970). Cleavage of structural proteins during the assembly of the head of bacteriophage T4. Nature *227*, 680–685.

Lee, A.Y., and Chung, S.S. (1999). Contributions of polyol pathway to oxidative stress in diabetic cataract. FASEB J. Off. Publ. Fed. Am. Soc. Exp. Biol. *13*, 23–30.

Like, A.A., and Rossini, A.A. (1976). Streptozotocin-induced pancreatic insulitis: new model of diabetes mellitus. Science *193*, 415–417.

Lo, T.W., Westwood, M.E., McLellan, A.C., Selwood, T., and Thornalley, P.J. (1994). Binding and modification of proteins by methylglyoxal under physiological conditions. A kinetic and mechanistic study with N alpha-acetylarginine, N alpha-acetylcysteine, and N alpha-acetyllysine, and bovine serum albumin. J. Biol. Chem. *269*, 32299–32305.

Lonn, E., Yusuf, S., Hoogwerf, B., Pogue, J., Yi, Q., Zinman, B., Bosch, J., Dagenais, G., Mann, J.F.E., and Gerstein, H.C. (2002). Effects of Vitamin E on Cardiovascular and Microvascular Outcomes in High-Risk Patients With Diabetes: Results of the HOPE Study and MICRO-HOPE Substudy. Diabetes Care *25*, 1919–1927.

References

Lowry, O.H., Rosebrough, N.J., Farr, A.L., and Randall, R.J. (1951). Protein measurement with the Folin phenol reagent. J. Biol. Chem. *193*, 265–275.

Lukic, I.K., Humpert, P.M., Nawroth, P.P., and Bierhaus, A. (2008). The RAGE pathway: activation and perpetuation in the pathogenesis of diabetic neuropathy. Ann. N. Y. Acad. Sci. *1126*, 76–80.

Madsen-Bouterse, S., Mohammad, G., and Kowluru, R.A. (2010). Glyceraldehyde-3-Phosphate Dehydrogenase in Retinal Microvasculature: Implications for the Development and Progression of Diabetic Retinopathy. Investig. Opthalmology Vis. Sci. *51*, 1765.

Malaguti, C., La Guardia, P.G., Leite, A.C.R., Oliveira, D.N., de Lima Zollner, R.L., Catharino, R.R., Vercesi, A.E., and Oliveira, H.C.F. (2014). Oxidative stress and susceptibility to mitochondrial permeability transition precedes the onset of diabetes in autoimmune non-obese diabetic mice. Free Radic. Res. *48*, 1494–1504.

Maruthur, N.M., Tseng, E., Hutfless, S., Wilson, L.M., Suarez-Cuervo, C., Berger, Z., Chu, Y., Iyoha, E., Segal, J.B., and Bolen, S. (2016). Diabetes Medications as Monotherapy or Metformin-Based Combination Therapy for Type 2 Diabetes: A Systematic Review and Meta-analysis. Ann. Intern. Med. *164*, 740.

Maruyama, W., Oya-Ito, T., Shamoto-Nagai, M., Osawa, T., and Naoi, M. (2002). Glyceraldehyde-3-phospate dehydrogenase is translocated into nuclei through Golgi apparatus during apoptosis induced by 6-hydroxydopamine in human dopaminergic SH-SY5Y cells. Neurosci. Lett. *321*, 29–32.

McCord, J.M., and Fridovich, I. (1969). Superoxide dismutase. An enzymic function for erythrocuprein (hemocuprein). J. Biol. Chem. *244*, 6049–6055.

Mills, G.C. (1957). Hemoglobin catabolism. I. Glutathione peroxidase, an erythrocyte enzyme which protects hemoglobin from oxidative breakdown. J. Biol. Chem. *229*, 189–197.

Misu, H., Takamura, T., Matsuzawa, N., Shimizu, A., Ota, T., Sakurai, M., Ando, H., Arai, K., Yamashita, T., Honda, M., et al. (2007). Genes involved in oxidative phosphorylation are coordinately upregulated with fasting hyperglycaemia in livers of patients with type 2 diabetes. Diabetologia *50*, 268–277.

Mitchell, P. (1975). The protonmotive Q cycle: a general formulation. FEBS Lett. *59*, 137–139.

Miyamoto, S., Hsu, C.-C., Hamm, G., Darshi, M., Diamond-Stanic, M., Declèves, A.-E., Slater, L., Pennathur, S., Stauber, J., Dorrestein, P.C., et al. (2016). Mass Spectrometry Imaging

References

Reveals Elevated Glomerular ATP/AMP in Diabetes/obesity and Identifies Sphingomyelin as a Possible Mediator. EBioMedicine *7*, 121–134.

Muller, F., Crofts, A.R., and Kramer, D.M. (2002). Multiple Q-cycle bypass reactions at the Qo site of the cytochrome bc1 complex. Biochemistry (Mosc.) *41*, 7866–7874.

Muller, F.L., Liu, Y., and Van Remmen, H. (2004). Complex III Releases Superoxide to Both Sides of the Inner Mitochondrial Membrane. J. Biol. Chem. *279*, 49064–49073.

Müller-Stich, B.P., Fischer, L., Kenngott, H.G., Gondan, M., Senft, J., Clemens, G., Nickel, F., Fleming, T., Nawroth, P.P., and Büchler, M.W. (2013). Gastric Bypass Leads to Improvement of Diabetic Neuropathy Independent of Glucose Normalization—Results of a Prospective Cohort Study (DiaSurg 1 Study): Ann. Surg. *258*, 760–766.

de Murcia, J.M., Niedergang, C., Trucco, C., Ricoul, M., Dutrillaux, B., Mark, M., Oliver, F.J., Masson, M., Dierich, A., LeMeur, M., et al. (1997). Requirement of poly(ADP-ribose) polymerase in recovery from DNA damage in mice and in cells. Proc. Natl. Acad. Sci. U. S. A. *94*, 7303–7307.

Murphy, M.P. (2009). How mitochondria produce reactive oxygen species. Biochem. J. *417*, 1–13.

Naderi, R., Mohaddes, G., Mohammadi, M., Ghaznavi, R., Ghyasi, R., and Vatankhah, A.M. (2015). Voluntary Exercise Protects Heart from Oxidative Stress in Diabetic Rats. Adv. Pharm. Bull. *5*, 231–236.

Nakamura, J., Kato, K., Hamada, Y., Nakayama, M., Chaya, S., Nakashima, E., Naruse, K., Kasuya, Y., Mizubayashi, R., Miwa, K., et al. (1999). A protein kinase C-beta-selective inhibitor ameliorates neural dysfunction in streptozotocin-induced diabetic rats. Diabetes *48*, 2090–2095.

Nakhoul, N., and Batuman, V. (2011). Role of Proximal Tubules in the Pathogenesis of Kidney Disease. In Contributions to Nephrology, G.A. Herrera, ed. (Basel: KARGER), pp. 37–50.

Nam, J.S., Cho, M.H., Lee, G.T., Park, J.S., Ahn, C.W., Cha, B.S., Lim, S.K., Kim, K.R., Ha, H.J., and Lee, H.C. (2008). The activation of NF-κB and AP-1 in peripheral blood mononuclear cells isolated from patients with diabetic nephropathy. Diabetes Res. Clin. Pract. *81*, 25–32.

Nawroth, P., Rudofsky, G., and Humpert, P. (2010). Have We Understood Diabetes? New Tasks for Diagnosis and Therapy. Exp. Clin. Endocrinol. Amp Diabetes *118*, 1–3.

References

Neubert, P., Halim, A., Zauser, M., Essig, A., Joshi, H.J., Zatorska, E., Larsen, I.S.B., Loibl, M., Castells-Ballester, J., Aebi, M., et al. (2016). Mapping the *O* -Mannose Glycoproteome in *Saccharomyces cerevisiae*. Mol. Cell. Proteomics *15*, 1323–1337.

Nguyen, T., Nioi, P., and Pickett, C.B. (2009). The Nrf2-Antioxidant Response Element Signaling Pathway and Its Activation by Oxidative Stress. J. Biol. Chem. *284*, 13291–13295.

Nicholls, C., Li, H., and Liu, J.-P. (2012). GAPDH: A common enzyme with uncommon functions: New functions of GAPDH. Clin. Exp. Pharmacol. Physiol. *39*, 674–679.

Obrosova, I.G., Li, F., Abatan, O.I., Forsell, M.A., Komjati, K., Pacher, P., Szabo, C., and Stevens, M.J. (2004). Role of Poly(ADP-Ribose) Polymerase Activation in Diabetic Neuropathy. Diabetes *53*, 711–720.

Oh, G.-S., Kim, H.-J., Choi, J.-H., Shen, A., Choe, S.-K., Karna, A., Lee, S.H., Jo, H.-J., Yang, S.-H., Kwak, T.H., et al. (2014). Pharmacological activation of NQO1 increases NAD+ levels and attenuates cisplatin-mediated acute kidney injury in mice. Kidney Int. *85*, 547–560.

Palsamy, P., and Subramanian, S. (2011). Resveratrol protects diabetic kidney by attenuating hyperglycemia-mediated oxidative stress and renal inflammatory cytokines via Nrf2–Keap1 signaling. Biochim. Biophys. Acta BBA - Mol. Basis Dis. *1812*, 719–731.

Peterson, L.R. (2004). Effect of Obesity and Insulin Resistance on Myocardial Substrate Metabolism and Efficiency in Young Women. Circulation *109*, 2191–2196.

Peterson, L.R., Herrero, P., McGill, J., Schechtman, K.B., Kisrieva-Ware, Z., Lesniak, D., and Gropler, R.J. (2008). Fatty Acids and Insulin Modulate Myocardial Substrate Metabolism in Humans With Type 1 Diabetes. Diabetes *57*, 32–40.

Phillips, S.A., and Thornalley, P.J. (1993). The formation of methylglyoxal from triose phosphates. Investigation using a specific assay for methylglyoxal. Eur. J. Biochem. FEBS *212*, 101–105.

Plantinga, L.C., Crews, D.C., Coresh, J., Miller, E.R., Saran, R., Yee, J., Hedgeman, E., Pavkov, M., Eberhardt, M.S., Williams, D.E., et al. (2010). Prevalence of Chronic Kidney Disease in US Adults with Undiagnosed Diabetes or Prediabetes. Clin. J. Am. Soc. Nephrol. *5*, 673–682.

Prochaska, H.J., and Santamaria, A.B. (1988). Direct measurement of NAD(P)H:quinone reductase from cells cultured in microtiter wells: A screening assay for anticarcinogenic enzyme inducers. Anal. Biochem. *169*, 328–336.

References

Rabbani, N., and Thornalley, P.J. (2011). Glyoxalase in diabetes, obesity and related disorders. Semin. Cell Dev. Biol. *22*, 309–317.

Rabbani, N., and Thornalley, P.J. (2012). Methylglyoxal, glyoxalase 1 and the dicarbonyl proteome. Amino Acids *42*, 1133–1142.

Rabbani, N., and Thornalley, P.J. (2014). Measurement of methylglyoxal by stable isotopic dilution analysis LC-MS/MS with corroborative prediction in physiological samples. Nat. Protoc. *9*, 1969–1979.

Ray, P.D., Huang, B.-W., and Tsuji, Y. (2012). Reactive oxygen species (ROS) homeostasis and redox regulation in cellular signaling. Cell. Signal. *24*, 981–990.

Raza, H., Prabu, S.K., John, A., and Avadhani, N.G. (2011). Impaired mitochondrial respiratory functions and oxidative stress in streptozotocin-induced diabetic rats. Int. J. Mol. Sci. *12*, 3133–3147.

Raza, H., John, A., and Howarth, F.C. (2015). Increased Oxidative Stress and Mitochondrial Dysfunction in Zucker Diabetic Rat Liver and Brain. Cell. Physiol. Biochem. *35*, 1241–1251.

Ristow, M., and Schmeisser, K. (2014). Mitohormesis: Promoting Health and Lifespan by Increased Levels of Reactive Oxygen Species (ROS). Dose-Response *12*, 288–341.

Ristow, M., Zarse, K., Oberbach, A., Kloting, N., Birringer, M., Kiehntopf, M., Stumvoll, M., Kahn, C.R., and Bluher, M. (2009). Antioxidants prevent health-promoting effects of physical exercise in humans. Proc. Natl. Acad. Sci. *106*, 8665–8670.

Rosca, M.G., Mustata, T.G., Kinter, M.T., Ozdemir, A.M., Kern, T.S., Szweda, L.I., Brownlee, M., Monnier, V.M., and Weiss, M.F. (2005). Glycation of mitochondrial proteins from diabetic rat kidney is associated with excess superoxide formation. Am. J. Physiol. Renal Physiol. *289*, F420–F430.

Ross, D., and Siegel, D. (2004). NAD(P)H:quinone oxidoreductase 1 (NQO1, DT-diaphorase), functions and pharmacogenetics. Methods Enzymol. *382*, 115–144.

Rushworth, S.A., MacEwan, D.J., and O'Connell, M.A. (2008). Lipopolysaccharide-induced expression of NAD(P)H:quinone oxidoreductase 1 and heme oxygenase-1 protects against excessive inflammatory responses in human monocytes. J. Immunol. Baltim. Md 1950 *181*, 6730–6737.

References

Sadi, G., Baloğlu, M.C., and Pektaş, M.B. (2015). Differential Gene Expression in Liver Tissues of Streptozotocin-Induced Diabetic Rats in Response to Resveratrol Treatment. PLOS ONE *10*, e0124968.

Sam, F., Kerstetter, D.L., Pimental, D.R., Mulukutla, S., Tabaee, A., Bristow, M.R., Colucci, W.S., and Sawyer, D.B. (2005). Increased Reactive Oxygen Species Production and Functional Alterations in Antioxidant Enzymes in Human Failing Myocardium. J. Card. Fail. *11*, 473–480.

Sarewicz, M., Borek, A., Cieluch, E., Świerczek, M., and Osyczka, A. (2010). Discrimination between two possible reaction sequences that create potential risk of generation of deleterious radicals by cytochrome bc1. Biochim. Biophys. Acta BBA - Bioenerg. *1797*, 1820–1827.

Schleicher, E.D., and Weigert, C. (2000). Role of the hexosamine biosynthetic pathway in diabetic nephropathy. Kidney Int. *58*, S13–S18.

Schmeisser, K., Mansfeld, J., Kuhlow, D., Weimer, S., Priebe, S., Heiland, I., Birringer, M., Groth, M., Segref, A., Kanfi, Y., et al. (2013). Role of sirtuins in lifespan regulation is linked to methylation of nicotinamide. Nat. Chem. Biol. *9*, 693–700.

Schmid, A.I., Szendroedi, J., Chmelik, M., Krssak, M., Moser, E., and Roden, M. (2011). Liver ATP Synthesis Is Lower and Relates to Insulin Sensitivity in Patients With Type 2 Diabetes. Diabetes Care *34*, 448–453.

Shen, X., Zheng, S., Metreveli, N.S., and Epstein, P.N. (2006). Protection of cardiac mitochondria by overexpression of MnSOD reduces diabetic cardiomyopathy. Diabetes *55*, 798–805.

Sim Choi, H., Woo Kim, J., Cha, Y., and Kim, C. (2006). A Quantitative Nitroblue Tetrazolium Assay for Determining Intracellular Superoxide Anion Production in Phagocytic Cells. J. Immunoassay Immunochem. *27*, 31–44.

Spranger, J., Kroke, A., Mohlig, M., Hoffmann, K., Bergmann, M.M., Ristow, M., Boeing, H., and Pfeiffer, A.F.H. (2003). Inflammatory Cytokines and the Risk to Develop Type 2 Diabetes: Results of the Prospective Population-Based European Prospective Investigation into Cancer and Nutrition (EPIC)-Potsdam Study. Diabetes *52*, 812–817.

Strother, R.M., Thomas, T.G., Otsyula, M., Sanders, R.A., and Watkins, J.B. (2001). Characterization of oxidative stress in various tissues of diabetic and galactose-fed rats. Int. J. Exp. Diabetes Res. *2*, 211–216.

References

Svingen, T., Letting, H., Hadrup, N., Hass, U., and Vinggaard, A.M. (2015). Selection of reference genes for quantitative RT-PCR (RT-qPCR) analysis of rat tissues under physiological and toxicological conditions. PeerJ *3*, e855.

Tan, A.L.Y., Sourris, K.C., Harcourt, B.E., Thallas-Bonke, V., Penfold, S., Andrikopoulos, S., Thomas, M.C., O'Brien, R.C., Bierhaus, A., Cooper, M.E., et al. (2010). Disparate effects on renal and oxidative parameters following RAGE deletion, AGE accumulation inhibition, or dietary AGE control in experimental diabetic nephropathy. Am. J. Physiol. Renal Physiol. *298*, F763–F770.

Thornalley, P.J. (1988). Modification of the glyoxalase system in human red blood cells by glucose in vitro. Biochem. J. *254*, 751–755.

Thornalley, P.J. (2003). Glyoxalase I--structure, function and a critical role in the enzymatic defence against glycation. Biochem. Soc. Trans. *31*, 1343–1348.

Thornalley, P.J., and Rabbani, N. (2014). Assay of methylglyoxal and glyoxal and control of peroxidase interference. Biochem. Soc. Trans. *42*, 504–510.

Tristan, C., Shahani, N., Sedlak, T.W., and Sawa, A. (2011). The diverse functions of GAPDH: Views from different subcellular compartments. Cell. Signal. *23*, 317–323.

Tukey, J.W. (1977). Exploratory data analysis (Reading, Mass: Addison-Wesley Pub. Co).

Tuttle, K.R., McGill, J.B., Haney, D.J., Lin, T.E., Anderson, P.W., and for the PKC-DRS, PKC-DMES, and PKC-DRS 2 Study Groups (2007). Kidney Outcomes in Long-Term Studies of Ruboxistaurin for Diabetic Eye Disease. Clin. J. Am. Soc. Nephrol. *2*, 631–636.

Tuttle, K.R., McGill, J.B., Bastyr, E.J., Poi, K.K., Shahri, N., and Anderson, P.W. (2015). Effect of Ruboxistaurin on Albuminuria and Estimated GFR in People With Diabetic Peripheral Neuropathy: Results From a Randomized Trial. Am. J. Kidney Dis. *65*, 634–636.

UKPDS Study Group (1998). Intensive blood-glucose control with sulphonylureas or insulin compared with conventional treatment and risk of complications in patients with type 2 diabetes (UKPDS 33). UK Prospective Diabetes Study (UKPDS) Group. Lancet Lond. Engl. *352*, 837–853.

Vander Jagt, D.L. (1993). Glyoxalase II: molecular characteristics, kinetics and mechanism. Biochem. Soc. Trans. *21*, 522–527.

Vander Jagt, D.L. (2008). Methylglyoxal, diabetes mellitus and diabetic complications. Drug Metabol. Drug Interact. *23*, 93–124.

References

VanderJagt, D.J., Harrison, J.M., Ratliff, D.M., Hunsaker, L.A., and Vander Jagt, D.L. (2001). Oxidative stress indices in IDDM subjects with and without long-term diabetic complications. Clin. Biochem. *34*, 265–270.

Ventura, M., Mateo, F., Serratosa, J., Salaet, I., Carujo, S., Bachs, O., and Pujol, M.J. (2010). Nuclear translocation of glyceraldehyde-3-phosphate dehydrogenase is regulated by acetylation. Int. J. Biochem. Cell Biol. *42*, 1672–1680.

Vial, G., Le Guen, M., Lamarche, F., Detaille, D., Cottet-Rousselle, C., Demaison, L., Hininger-Favier, I., Theurey, P., Crouzier, D., Debouzy, J., et al. (2016). Liver mitochondrial function in ZDF rats during the early stages of diabetes disease. Physiol. Rep. *4*, e12686.

Vinogradov, A.D., and Grivennikova, V.G. (2005). Generation of superoxide-radical by the NADH:ubiquinone oxidoreductase of heart mitochondria. Biochemistry (Mosc.) *70*, 120–127.

Widlansky, M.E., Wang, J., Shenouda, S.M., Hagen, T.M., Smith, A.R., Kizhakekuttu, T.J., Kluge, M.A., Weihrauch, D., Gutterman, D.D., and Vita, J.A. (2010). Altered mitochondrial membrane potential, mass, and morphology in the mononuclear cells of humans with type 2 diabetes. Transl. Res. J. Lab. Clin. Med. *156*, 15–25.

Will, Y., Hynes, J., Ogurtsov, V.I., and Papkovsky, D.B. (2007). Analysis of mitochondrial function using phosphorescent oxygen-sensitive probes. Nat. Protoc. *1*, 2563–2572.

Wright, J.J., Kim, J., Buchanan, J., Boudina, S., Sena, S., Bakirtzi, K., Ilkun, O., Theobald, H.A., Cooksey, R.C., Kandror, K.V., et al. (2008). Mechanisms for increased myocardial fatty acid utilization following short-term high-fat feeding. Cardiovasc. Res. *82*, 351–360.

Xia, P., Inoguchi, T., Kern, T.S., Engerman, R.L., Oates, P.J., and King, G.L. (1994). Characterization of the mechanism for the chronic activation of diacylglycerol-protein kinase C pathway in diabetes and hypergalactosemia. Diabetes *43*, 1122–1129.

Ye, G., Metreveli, N.S., Donthi, R.V., Xia, S., Xu, M., Carlson, E.C., and Epstein, P.N. (2004). Catalase Protects Cardiomyocyte Function in Models of Type 1 and Type 2 Diabetes. Diabetes *53*, 1336–1343.

Zhang, J.-Z., Gao, L., Widness, M., Xi, X., and Kern, T.S. (2003). Captopril inhibits glucose accumulation in retinal cells in diabetes. Invest. Ophthalmol. Vis. Sci. *44*, 4001–4005.

8 Appendix

Table 6. ATP production and levels in heart, liver and kidney of different diabetic models

Model	Induction of diabetes	Duration[*] weeks	Result	Substrate	Reference
Heart					
♂ db/db	genetic T2D	4	↓ in permeabilized tissue	malate	(Boudina et al., 2007)
♂ wild type mice	low dose STZ[2]	4	↓ in permeabilized tissue	malate	(Bugger et al., 2012)
♂ Ins2^{+/-} Akita mice	genetic T1D	6	↓ in isolated mt	succinate	(Bugger et al., 2009)
♂ Ins2^{+/-} Akita mice	genetic T1D	6	↔ in isolated mt	malate	(Bugger et al., 2009)
Liver					
♂ Ins2^{+/-} Akita mice	genetic T1D	6	↔ in isolated mt	malate or succinate	(Bugger et al., 2009)
♂ Zucker rat	genetic T2D	30	↓ liver ATP content	-	(Raza et al., 2015)
♀, ♂ patients	T2D	-	↓ATP turnover	MRS	(Schmid et al., 2011)
♂ C57BL/6J	HFD	30 (HFD)	↑ in isolated mt	malate	(Guo et al., 2013)
Kidney					
♂ Sprague-Dawley rats	single dose STZ	4-32	↓ renal ATP content	-	(Coughlan et al., 2016)
♂ Ins2^{+/-} Akita mice	genetic T1D	6	↔in isolated mt	malate or succinate	(Bugger et al., 2009)
♂ C57BL/6J	low dose STZ[2]	24	↓ mt ATP production	malate	(Tan et al., 2010)
♂ Ins2^{+/-} Akita mice	genetic T1D	20	↑glomeruli ATP content ↓ medula ATP content		(Miyamoto et al., 2016)

[1] of diabetes

[2] low dose STZ for 5 consecutive days

mitochondria (mt), high fat diet (HFD), magnetic resonance spectroscopy (MRS)

Table 7. O$_2$ consumption in heart, liver and kidney of different diabetic models

Model	Induction of diabetes	Duration[*] weeks	Result	Substrate	Reference
Heart					
♂ db/db mice	genetic T2D	4	↓ in permeabilized tissue	malate	(Boudina et al., 2007)
♂ wild type mice	low dose STZ[2]	4	↔ in permeabilized tissue	malate	(Bugger et al., 2012)
♂ Ins2^{+/-} Akita mice	genetic T1D	6	↓ in isolated mt	malate or succinate	(Bugger et al., 2009)
♂ OVE26 mice	genetic T1D	8	↓ in isolated mt	malate	(Shen et al., 2006)
Liver					
♂ Ins2^{+/-} Akita mice	genetic T1D	6	↔ in isolated mt	malate or succinate	(Bugger et al., 2009)
♂ Sprague-Dawley rats	single dose STZ	8	↑ in isolated mt	succinate	(Raza et al., 2011)
ZDF fa/fa rats	genetic T2D	11, 14	↔ in isolated mt	malate or succinate	(Vial et al., 2016)
♂ C57BL/6J mice	HFD	30 (HFD)	↑ in isolated mt	malate or succinate	(Guo et al., 2013)
♀ NOD mice	genetic T1D	4 – 25 weeks of age	↔ in isolated mt in non-diabetic, pre-diabetic and diabetic stage	malate	(Malaguti et al., 2014)
Kidney					
♂ Sprague-Dawley rats	single dose STZ	4-32	↑ in isolated mt (starting from week 16)	malate	(Coughlan et al., 2016)
♂ Ins2^{+/-} Akita mice	genetic T1D	6	↑ in isolated mt	malate or succinate	(Bugger et al., 2009)
♂ Lewis rats	single dose STZ	8, 24, 48	↔ in isolated mt, week 8 ↓ in isolated mt, week 24 and 48	malate	(Rosca et al., 2005)

[1] of diabetes

[2] low dose STZ for 5 consecutive days

mitochondria (mt), high fat diet (HFD)

Table 8. ROS production in heart, liver and kidney of different diabetic models

Model	Induction of diabetes	Duration[*] weeks	Result	Substrate	Reference
Heart					
♂ db/db mice	genetic T2D	4	↑ mt H_2O_2 production	succinate + Omy	(Boudina et al., 2007)
♂ wild type mice	low dose STZ[2]	4	↔ H_2O_2 production in permeabilized fibers	succinate	(Bugger et al., 2012)
♂ Lewis rats	single dose STZ	10	↑ mt H_2O_2 production	succinate	(Rosca et al., 2005)
Liver					
♂ Sprague-Dawley rats	single dose STZ	8	↑ in isolated mt	-	(Raza et al., 2011)
♂ Zucker rat	genetic T2D	30	↓ total and membrane bound ROS production ↔ mt ROS production	-	(Raza et al., 2015)
ZDF fa/fa rats	genetic T2D	11, 14	↓ mt H_2O_2 production at 14 weeks	malate or succinate	(Vial et al., 2016)
♀ NOD mice	genetic T1D	4 – 25 weeks of age	↑ mt H_2O_2 and ROS production in non-diabetic stage ↔ mt H_2O_2 and ROS production in pre-diabetic and diabetic stage	malate	(Malaguti et al., 2014)
Kidney					
♂ Sprague-Dawley rats	single dose STZ	4-32	↑ mt H_2O_2 production (starting from week 8)	malate	(Coughlan et al., 2016)
♂ Sprague-Dawley rats	single dose STZ	12	↑ mt H_2O_2 production	malate	(de Cavanagh et al., 2008)
♂ C57BL/6 mice	low dose STZ[2]	24	↓ O_2^- production *in vivo*	real-time imaging	(Dugan et al., 2013)
♂ C57BL/6 mice	low dose STZ[2]	24	↓ mt H_2O_2 production	malate or succinate	(Dugan et al., 2013)
♂ Ins2$^{+/-}$ Akita mice	genetic T1D	10	↑ glomerular O_2^- level	histo-chemistry	(Fujita et al., 2012)
♂ Ins2$^{+/-}$ Akita mice	genetic T1D	12	↑ increase in ROS levels in the tissue	histo-chemistry	(Abdo et al., 2014)
♂ Wistar rats	single dose STZ	4	↑ mt H_2O_2 production in tissue homogenate	cytochrome reduction	(Palsamy and Subramanian, 2011)

[1] of diabetes

[2] low dose STZ for 5 consecutive days

mitochondria (mt)

Table 9. SOD level and activity in heart, liver and kidney of different diabetic models

Model	Induction of diabetes	Duration[*] weeks	Result	Reference
Heart				
Wistar rats	single dose alloxan	8	↓ SOD1activity	(Aliciguzel et al., 2003)
♂ db/db mice	genetic T2D	4	↑ SOD2 protein level	(Boudina et al., 2007)
♂ Sprague-Dawley rats	single dose STZ	4	↑ total SOD activity	(Strother et al., 2001)
♂ Wistar rats	single dose STZ	24	↔ total SOD activity	(Naderi et al., 2015)
♀ Wistar rats	single dose alloxan	12	↔ SOD1 activity	(Godin et al., 1988)
Liver				
Wistar rats	single dose alloxan	8	↔ SOD1 activity	(Aliciguzel et al., 2003)
♂ Sprague-Dawley rats	single dose STZ	1, 6	↑ total SOD and SOD1 acitivity ↔ SOD2 activity (starting form week 1)	(Kakkar et al., 1998)
♂ C57BL/6N mice	low dose STZ[2]	8	↔ SOD2 protein level	(Franko et al., 2014)
♀ Wistar rats	single dose alloxan	12	↓ SOD1 activity	(Godin et al., 1988)
♂ Wistar rats	single dose alloxan	4	↓ *Sod1* and *Sod2* mRNA level ↑ SOD1 protein level/ acitivity ↔ SOD2 protein level/ acitivity	(Sadi et al., 2015)
Kidney				
♂ Sprague-Dawley rats	single dose STZ	4-32	↓ SOD2 activity (starting from week 8)	(Coughlan et al., 2016)
♂ Sprague-Dawley rats	single dose STZ	12	↓ SOD2 activity	(de Cavanagh et al., 2008)
Wistar rats	single dose alloxan	8	↔ SOD1 activity	(Aliciguzel et al., 2003)
♂ db/db mice	genetic T2D	18	↑ SOD1 protein level in the glomeruli ↓ SOD1 protein level in the tubules ↔ SOD1 activity in cortex and glomeruli	(Barati et al., 2007)
♂ db/db mice	genetic T2D	16	↔ SOD1 and SOD2 activity in renal cortex	(DeRubertis et al., 2004)
♂ Ins2^{+/-} Akita mice	genetic T1D	10	↔ SOD1, SOD2, SOD3 protein level ↓ total SOD activity	(Fujita et al., 2012)
♂ Sprague-Dawley rats	single dose STZ	4	↑ total SOD activity	(Strother et al., 2001)

[1] of diabetes

[2] low dose STZ for 5 consecutive days

Table 10. CAT level and activity in heart, liver and kidney of different diabetic models

Model	Induction of diabetes	Duration[*] weeks	Result	Reference
Heart				
Wistar rats	single dose alloxan	8	↓ CAT activity	(Aliciguzel et al., 2003)
♀ Wistar rats	single dose alloxan	12	↑ CAT activity	(Godin et al., 1988)
♀, ♂ OVE26 mice	genetic T1D	20	↑ CAT mRNA	(Ye et al., 2004)
♂ Wistar rats	single dose STZ	24	↔ CAT activity	(Naderi et al., 2015)
Liver				
Wistar rats	single dose alloxan	8	↑ CAT activity	(Aliciguzel et al., 2003)
♂ Sprague-Dawley rats	single dose STZ	1, 6	↑ CAT activity (starting form week 1)	(Kakkar et al., 1998)
♂ Sprague-Dawley rats	single dose STZ	4	↓ CAT activity	(Strother et al., 2001)
♂ Zucker rat	genetic T2D	30	↔ CAT activity	(Raza et al., 2015)
♀ Wistar rats	single dose alloxan	12	↓ CAT activity	(Godin et al., 1988)
Kidney				
Wistar rats	single dose alloxan	8	↑ CAT activity	(Aliciguzel et al., 2003)
♂ db/db mice	genetic T2D	16	↔ cortical CAT activity	(DeRubertis et al., 2004)
♀ Wistar rats	single dose alloxan	12	↓ CAT activity	(Godin et al., 1988)
♂ Ins2$^{+/-}$ Akita mice	genetic T1D	12	↓ Cat mRNA/ activity	(Abdo et al., 2014)

[1] of diabetes

9 Personal Publications

Publications

- Mendler, M., Riedinger, C., Schlotterer A., **Volk, N.**, Fleming, T., Herzig, S., Nawroth, P.P., Morcos, M. (2016). Blocking ins-7 signalling in high glucose exposed Caenorhabditis elegans protects from reactive metabolites, preserves neuronal function, and prolongs lifespan. Journal of Diabetes and Its Complications. In press.

Manuscripts in preparation

- **<u>Volk, N.</u>**, Kliemank, E., Poschet, G., Kynast, K., Herpel, E., Fleming, T.H., Nawroth, P.P. (2016). Elevated glucose levels do not activate the pathways of hyperglycemic damage in the kidney of type 1 and type 2 diabetic mice. In preparation for submission to Diabetes.

- Spanidis, I., Hidmark, A., Fleming, T.H., **Volk, N.**, Eckstein, V., Gröner, J.B., Kopf S., Nawroth, P.P., Oikonomou, D. (2016). External muscle stimulation differentiates circulating haemotopoietic stem cells in diabetes patients. In preparation for submission.

- Micakovic, T., Papagiannarou, M., Clark, E., Peters, J., **Volk, N.,** Fleming, T., Alenina, N., Gröne, H.J., Hoffmann, S. (2016). Angiotensin II type 2 receptor localises to mitochondria of renal tubules and modifies mitochondrial function in early stage of type 1 diabetes in rats.

- Peters, V., et al. (2016). The antioxidant capacity of anserine and carnosine.

Conference proceedings

- **<u>Volk, N.,</u>** Fleming, T., Kliemank, E., Poschet, G., Nawroth, P.P. (2016). Glucose-induced increase in superoxide production is absent in the diabetic kidney – Nephropathy develops independent of the unifying theory. 3rd Heidelberg International Symposium on Diabetic Complications.

- Micakovic, T., Papagiannarou, M., Clark, E., Peters, J., **Volk, N.,** Fleming, T., Alenina, N., Gröne, H.J., Hoffmann, S. (2016). Angiotensin II type 2 receptor localises to mitochondria of renal tubules and modifies mitochondrial function in early stage of type 1 diabetes in rats. EASD, 52 – P 1041.

- Spanidis, I., Hidmark, A., Fleming, T.H., **Volk, N.**, Eckstein, V., Gröner, J.B., Kopf, S., Nawroth, P.P., Oikonomou, D. (2016). External muscle stimulation differentiates circulating haemotopoietic stem cells in diabetes patients. EASD, 52 – OP 160.

- Micakovic, T., Papagiannarou, M., Clark, E., **Volk, N.,** Fleming, T., Gröne, H.J., Hoffmann, S. (2016). Angiotensin II type 2 receptor (AT2R) localizes to mitochondria of renal tubules and modifies mitochondrial function in early stages of type 1 diabetes in rats. Diabetologie und Stoffwechsel, 11 - P146.

- Spanidis, I., Hidmark, A., Fleming, T., **Volk, N.**, Eckstein, V., Gröner, J.B., Kopf, S., Nawroth, P.P., Oikonomou, D. (2016). External muscle stimulation differentiates circulating hematopoietic stem cells in diabetes patients. Diabetologie und Stoffwechsel, 11-FV29.

Personal Publications

- **<u>Volk, N.,</u>** Fleming, T., Kliemank, E., Kynast, K., Herpel, E., Nawroth, P.P. (2015). Tissue-specific effects on mitochondrial dysfunction in type 2 diabetic mouse models. 2nd Heidelberg International Symposium on Diabetic Complications.

- **<u>Volk, N.,</u>** Fleming, T., Kliemank, E., Kynast, K., Herpel, E., Nawroth, P.P. (2015). Tissue-specific effects on mitochondrial dysfunction in type 2 diabetic mouse models. EASD, 51 - P1154.

- **<u>Volk, N.,</u>** Fleming, T., Kliemank, E., Nawroth, P.P. (2015). Organ-specific effects of diabetes on mitochondrial function. Diabetologie und Stoffwechsel, 10 - P66.

- Vittas, S., Fleming, T., Hidmark, A., Oikonomou, D., **Volk, N.**, Kopf, S., Nawroth, P.P. (2015). Pyruvate kinase isoenzyme M2 is increased in experimental diabetes and correlates with diabetic neuropathy in patients. Diabetologie und Stoffwechsel, 10 - P66.

- **<u>Volk, N.,</u>** Hidmark, A.S., de Villiers, E.M., Fleming, T.H., Nawroth, P.P. (2014). Tissue-Specific Effect on Mitochondrial Dysfunction in Type 1 and 2 Diabetic Mouse Models. 1st Heidelberg International Symposium on Diabetic Complications.

- **<u>Volk, N.,</u>** Hidmark, A.S., de Villiers, E.M., Fleming, T.H., Nawroth, P.P. (2014). Streptozotocin-induced diabetes does not affect mitochondrial structure and function. EASD, 50 - P1313.

- Vittas, S., Kopf, S., **Volk, N.**, Hidmark, A., Oikonomou, D., Fleming, T.H., Nawroth, P.P. (2014). Pyruvate kinase isoenzyme M2 shows increased expression in diabetes. EASD, 50 - P1314.

10 Curriculum Vitae

Personal Information

Name	**Nadine Volk**
Address	Lindenallee 21 64743 Beerfelden
Phone E-mail	+49 176 70325021 nadine.volk@med.uni-heidelberg.de
Date and place of birth	02.09.1986 in Eberbach am Neckar

Education

10/2016 – ongoing	**Institute of Pathology Heidelberg** Project Coordinator of the SFB 1118 Tissue Bank
02/2013 – 09/2016	**University Clinic Heidelberg** International Graduate School Diabetic Microvascular Complications (DIAMICOM) • Internal Medicine and Clinical Chemistry, Prof. Dr. Nawroth *Diabetes-induced mitochondrial changes are tissue- and model-dependent and elevated glucose levels do not activate the pathways of hyperglycemic damage in the kidney*
10/2010 - 10/2012	**Ruprecht-Karls University Heidelberg** Faculty of Bioscience, Major: Molecular and Cellular Biology **Master of Science** (1.4) • German Cancer Research Center, Prof. Dr. Rösl *The Role of Parkin and Pink in Mitochondrial Homeostasis and HPV-Induced Carcinogenesis*
10/2007 - 07/2010	**Ruprecht-Karls University Heidelberg** Faculty of Bioscience, Major: Molecular and Cellular Biology **Bachelor of Science** (1.6) • German Cancer Research Center, Prof. Dr. Rösl *Production and Characterization of Recombinant Interferon kappa in a Mammalian System*
09/1997 - 07/2006	**Hohenstaufen-Gymnasium Eberbach** Abitur (higher education entrance qualification) (1.2)

<u>Curriculum Vitae</u>

09/2011 - 11/2011	**Karolinska Institute, Sweden**

Traineeship

- Department of Oncology-Pathology, Prof. Dr. Grandér
  Development and Validation of a Screening System to Monitor STAT3 Transcriptional Activity in Cancer Cells

07/2010 - 09/2010	**Mahasarakam University, Thailand**

Traineeship

- Faculty of Science, Asst. Prof. Dr. Srivilaj
  Assistance in the theoretical and practical education of bachelor students

08/2006 - 08/2007	**Cultural Care Au pair**

Au pair in Monroe Township, NJ, USA

11 Acknowledgement